Adsorption of small polarisable molecules using mesoporous carbonaceous materials

Roxana Alina Milescu

MSc by Research

University of York

Chemistry

August 2017

Abstract

Discovered and first reported 11 years ago by the York Green Chemistry Centre of Excellence, Starbon® is carbonaceous mesoporous material derived from polysaccharides (starch or alginic acid). These renewable materials represent a greener, more efficient, cheaper and more selective alternative than other commercial options in reducing emissions from power stations, chemical and other large scale manufacturing plants. It has been shown that the Starbon® materials were successfully applied in chromatography, noble metals and large dye molecules adsorption. The next ambition is to utilize the unique textural properties and surface chemistry of the Starbon® for adsorption adsorption of small gas molecule. It is an interesting challenge because the microporosity is the key factor in small molecules adsorption and there is a little information about role of mesoporosity in this process.

Starbons® have much lower microporosities, but adsorb up to 65% more CO_2 than activated carbon. Furthermore, novel Starbons®-graphene composite materials developed during the project adsorb even more CO_2 due to their very microporous combination with graphene. During the project it has been demonstrated that the adsorption capacity of the micropore system to adsorb small molecules could be significantly increased in the presence of mesopore. This phenomenon has been shown on the example of adsorption of small polarizable molecules such as CO_2 and NH_3.

It has been found that carbonaceous materials could adsorb ammonia by micropores (reversible process) and chemically interact with their surface functional groups (irreversible process). The chemisorption of ammonia onto the Starbon® being correlated with the functionality surface and the temperature of the adsorption. Moreover, the NH_3 interaction with Starbons® led to new bio-based nitrile-containing mesoporous materials. The introduction of nitrogen is expected to improve CO_2 capture performance, heavy-metal binding, conductivity and catalytic activity, most notably in the metal-free oxidative reduction reaction.

Because Starbons® display a high adsorption of CO_2 and NH_3 there may be potential to use them in the adsorption of other small molecules, as NO_x, SO_x. Further research would need to take place in order to discover Starbon® potential in adsorption of these small molecules.

Contents

List of Figures

List of Tables

Acknowledgements

First of all, I would like to thank Professor James H Clark and Dr. Vitaliy Budarin for their enthusiastic supervision throughout the project.

I would also like to thank Mr. Paul Elliott for his day to day help and training in the lab and Maria Garcia for her constant help and information about Starbon® preparation.

I would like to thank Dr. Duncan MacQuarrie for his help in FTIR analysis, Dr. Andrew Hunt for his support and advice, James Shannon, Andrea Munoz and Jennifer Attard for our fruitful discussions about Starbon®

I would also like to thank Dr. Ian Ingram for helping me with writing my thesis.

I also thank to Meg Stark from Bioscience Technology Facility, Biology Dept, University of York for carrying out the SEM and TEM sections, Professor Maria-Magdalena Titirici from The School of Engineering and Materials Science, Queen Mary, University of London and David Morgan from National EPSRC XPS Users Service (NEXUS), Newcastle University for their help with the XPS analyses.

Finally, I would like to thank my family, all my friends from Green Chemistry department and my work manager Ben Morcombe for his support during my MSc, without whom it would not have been possible to complete my studies.

Declaration

I declare that this thesis is a presentation of original work and I am the sole author. This work has not previously been presented for an award at this, or any other, University. All sources are acknowledged as References.

1. Introduction

It is well known that the major pollutants from power stations and motor vehicles are CO_2, NO_x, CO and SO_x.[1] Emissions of such oxides as NO_x and SO_x lead to a complex series of chemical and physical transformations. These result in effects as the formation of ozone[2] as well as in the global troposphere,[3] acid deposition,[4] the formation of secondary particulate matter through gas/particle partitioning of the emitted chemical compounds and the atmospheric reaction products of NO_x, SO_2 and organosulfur compounds.[5,6,7,8,9] On the other side the presence of carbon dioxide in atmosphere has caused most of the Global Warming and its influence is expected to continue.[10] Furthermore, there are risks that these toxic molecules produced could provoke respiratory infections, heart disease, stroke and lung cancer (see Figure 1).[11]

Figure 1. Effects of CO_2, NO_x and SO_x pollution on human health

Between all the gases CO_2 and NH_3 adsorption were chosen in this study to research the chemistry of interaction between the Starbons® functionalities with an acidic and respectively a basic material. Carbon dioxide (CO_2) is considered as the most important greenhouse gas with the largest impact on climate change, due to burning of fossil fuels is becoming a serious environmental problem[12,13] and NH_3 and its derivatives are considered very dangerous for human and aquatic health. It has been recognized that the surface chemistry of activated carbon can strongly affect the adsorption capacity.[14] Due to acidic role of CO_2, it is expected that the introduction of Lewis bases onto the activated carbon surfaces to increase the CO_2 capture performance of these materials.[15] The amination of AC was found to be a suitable modification technique for obtaining efficient CO2 adsorbents.[16]

Methods to capture CO_2 include: chemical absorption, physical adsorption, cryogenic separation and membrane separation[17], but most of them are too expensive and / or not available on a large scale. Moreover, the aqueous amines were used as capture

agents for CO_2 and have had many disadvantages such as being corrosive, unstable to toxic by-products such as nitrosamines[18,19,20,21,22]One of the most used materials for adsorption is activated carbon AC. It has been successfully applied for air and water purification[23], dye removal[24] metal extraction[25] medicine, sewage treatment.[26,27,28] Due to their high surface area, availability, low cost and easy to regenerate[29] activated carbons were used in the past for adsorption of many poisons and it's well known for its ability to keep them away from the bloodstream.[30] The absorbers have been used to control the emission or to increase the concentration of VOCs to allow either destruction by incineration, or recovery by membrane or condenser to be economically feasible.[31]

The AC have important applications in gas purification (H_2S removal from biogas, CO_2 purification, hydrogen purification) and pollutant adsorption (solvent recovery, storage tank ventilation, Hg, dioxin and other trace contaminants removal from flue gas).[32] The pollutant is adsorbed on the surface (mostly the internal surface) of adsorbent material.[33] The process of major pollutants adsorption is reversible and therefore the adsorbents and can be reused (desorbed as part of regenerating the adsorbent) easily by heating or vacuum[34,35] In the past AC played an important role in trapping small volatile poisoning gases such as NH_3[36,37] and as well as malodorous compounds.[38,39]

The microporous (or sub-microporous) solids make the best adsorbents having the fast adsorption kinetics, big surface area, large pore volume, lower cost, potentially environmentally benign nature, and high thermal stability, all compared to other adsorbent such as zeolites,[40,41] activated carbon and metal–organic frameworks (MOFs).[42,43] However, one of the biggest problem of activated carbon is rate of desorption and desorption due to small diameter of micropore.

The newly discovered Starbons® materials are renewable, more efficient and selective alternative to other commercial options in trapping these gasses.
It has been found that introduction of nitrogen functional groups into the carbon surface made it better in CO_2 adsorption.[44-48]

Significant efforts are being made to create new environmentally benign materials and the biomass is often cheap, abundant, biodegradable and available from agricultural waste, food production and forestry by-products.

Starbons® made from biomass, including food waste and seaweed, were discovered and first reported 11 years ago by the York Green Chemistry Centre of Excellence.[49,50] With silica-based being the first reported mesoporous materials and it's need for templating to allow very specific structures[51,52] and with most of the commercially used carbons being microporous and hydrophobic, the newly discovered mesoporous Starbons® were developed without the need for a templating agent and avoiding the use of aggressive chemical processes.[53]

They are considered to be green and sustainable as they are made from renewable materials using a clean production process: the polysaccharides are gelated and freeze-dried to give a mesoporous aerogel that can be carbonised (300 – 800° C) to obtain a range of mesoporous materials with varying surface functionalities.[54] The carbonaceous microspheres typically present very low surface areas and porosity and need routes to introduce high surface area and (e.g. micro-, meso- and macro-) porosity.[55]

Carbons, depending on their structure, may have the added the advantage of being electrically conductive, making them potentially useful for applications in energy capture and storage.[56] With applications in optics, catalysis, drug delivery systems, coatings, cosmetics, bio-separation, diagnostics, gas-separation and nanotechnology they have also recently proven to be good adsorbers of metals [57] and small molecules such as CO_2.[58]

As the properties of various carbonaceous materials were studied, their surface functionality played an important role in their applicability. Research then focused on expanding the range of existing materials by functionalising their surfaces using more functionally starting materials or, by attaching other compounds onto the surfaces of already mesoporous materials. One such example is the introduction of nitrogen using ammonia as it has shown to improve heavy-metal binding, conductivity and catalytic activity, most notably in the metal-free oxidative reduction reaction[59,60,61,62] and the CO_2 capture performance of these materials.[15]

A sustainable future for carbon materials science and a clean environment are necessary and are taken into consideration new routes of obtaining new carbon materials derived from renewable resources, more sustainable variants of classical carbon materials (*e.g.*, activated carbons, carbon nanotubes, carbon aerogels).[63]

This project will aim to produce these bio-based materials whilst respecting a number of Green Chemistry rules:

- "Rule 1. *Prevention* ‘’- It is better to prevent waste than to treat or clean up waste after it has been created.
- ‘’Rule 2. *Atom Economy*’’- Synthetic methods should be designed to maximize the incorporation of all materials used in the process into the final product.
- "Rule 3. *Less Hazardous Chemical Syntheses"*- Wherever practicable, synthetic methodologies should be designed to use and generate substances that possess little or no toxicity to human health and the environment.
- "Rule 4. *Designing Safer Chemicals"* - Chemical products should be designed to preserve efficacy of function while reducing toxicity.

- "Rule 5. *Safer Solvents and Auxiliaries"* -The use of auxiliary substances (e.g., solvents, separation agents, etc.) should be made unnecessary wherever possible and innocuous when used.

- ‘’Rule 6. *Design for Energy Efficiency*’’- Energy requirements of chemical processes should be recognized for their environmental and economic impacts and should be minimized. If possible, synthetic methods should be conducted at ambient temperature and pressure.
- "Rule 7. *Use of Renewable Feedstocks"-* A raw material of feedstock should be renewable rather than depleting wherever technically and economically practicable.

- ‘’Rule 8. *Reduce Derivatives*’’- Unnecessary derivatization (use of blocking groups, protection/deprotection, temporary modification of physical/chemical processes) should be minimized or avoided if possible, because such steps require additional reagents and can generate waste.
- ‘’Rule 9. Catalysis - Catalytic reagents (as selective as possible) are superior to stoichiometric reagents.
- "Rule 10. *Design for Degradation"-* Chemical products should be designed so that at the end of their function they break down into innocuous degradation products and do not persist in the environment.

- "Rule 11. *Real- time analysis for Pollution Prevention"-* Analytical methodologies need to be further developed to allow for real-time, in-process monitoring and control prior to the formation of hazardous substances.

- "Rule 12. *Inherently Safer Chemistry for Accident Prevention"-* Substances and the form of a substance used in a chemical process should be chosen to minimize the potential for chemical accidents, including releases, explosions, and fires.[64]

2. Results and discussion

2.1. Preparation and characterisation of Starbon® materials

2.1.1. Polysaccharide-derived Starbons

Starbon® is a mesoporous carbonaceous material derived from polysaccharides (starch or alginic acid) which is both mesoporous and microporous, containing pores with diameters between 2 and 50 nm (Fig2)[65].

For many applications, it is desirable to control the pore size and the surface chemistry. For applications in chromatography[66] and catalysis[67,68], a mesoporous structure is preferred, and the presence of some micropores is unnecessary. However, for gas sorption applications, in our case carbon dioxide adsorption[54], the presence of micropore interconnected with mesopores is key.

Pore type	Pore size	Condensation mechanism	Type of adsorption
Micropore	<2 nm	Three-dimensional	Non-specific
Mesopore	≥2 ≤50 nm	Capillary	Specific
Macropore	>50 nm	No condensation	Non-specific

Figure 2. IUPAC definition of micro, meso and macropores

For this work, the method using tert-Butanol (TBA) and freeze-drying was chosen as it avoids the use of toluene, it's affordable and it preserves the large pores of the polysaccharide's structure when replaces the water, leaving large crystals.[54]

The freeze drying method, by contrast to the earliest method employing sulfolane, does not result in contamination of the final material (Fig 3).

The peaks highlighted at 1299 cm^{-1} and 1106 cm^{-1} are characteristics of residual toluene remaining after carbonisation when using sulfolane.

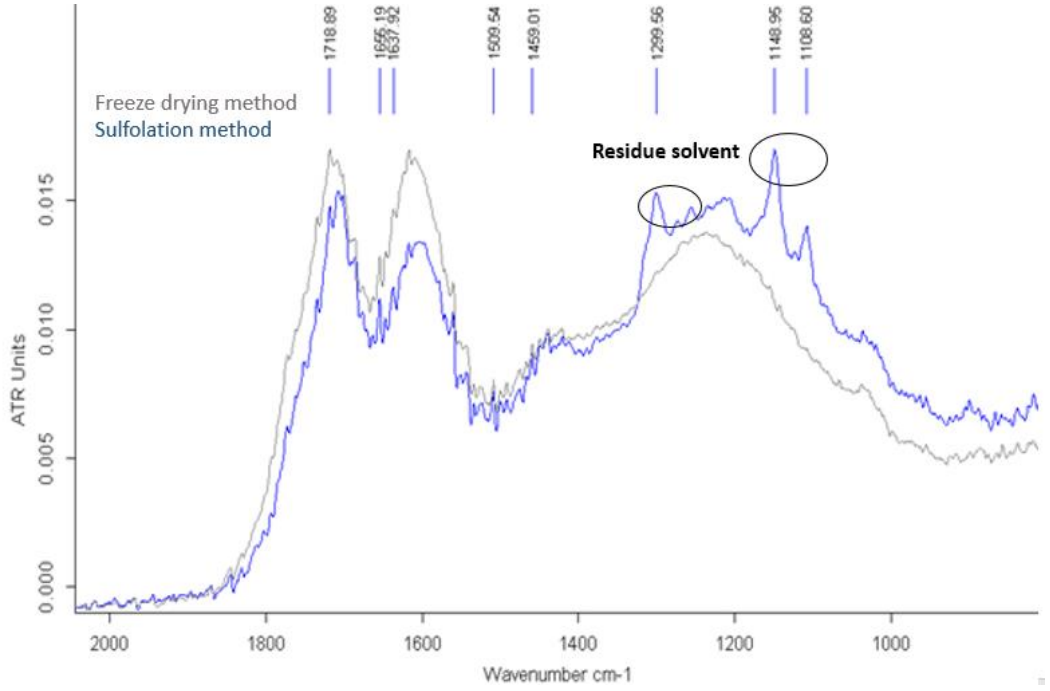

Figure 3. FTIR spectrum of Starbon materials produced by different methods and the presence of residue solvent in sulfolation method

All the expanded materials are white aerogels before carbonisation. As seen in Fig 4, a 100°C they become yellowish, but carbonised over 300°C they become dark brown-black material and black above that temperature:

Figure 4. Expanded starch and Starbon obtained at temperatures of 100 and 300 ℃

The pore-size distribution (Fig 5) indicates a predominance of mesopores with the volume and diameter of pores in the range 0.2-0.7 $cm^3 g^{-1}$ and 9-14 nm for starch derivatives and 0.3-0.9 $cm^3 g^{-1}$ and 6-13 nm for alginic acid derivatives.

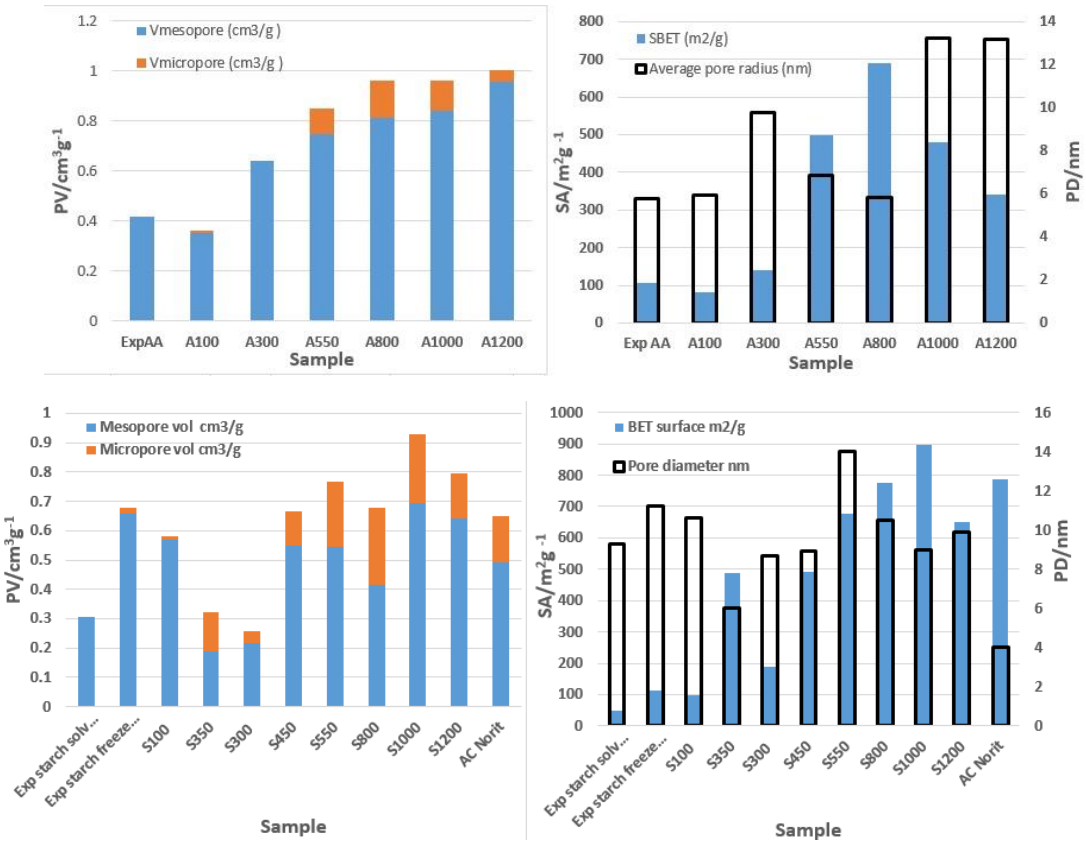

Figure 5. Comparison of textural properties of AC and mesoporous materials (Starbon and Algibon)

The total pore volume and the average pore diameter in the mesoporous region remain constant throughout the carbonisation process.[69] Above 300˚C micropores make a big difference in the total surface area, with a predominance of the mesopore region.

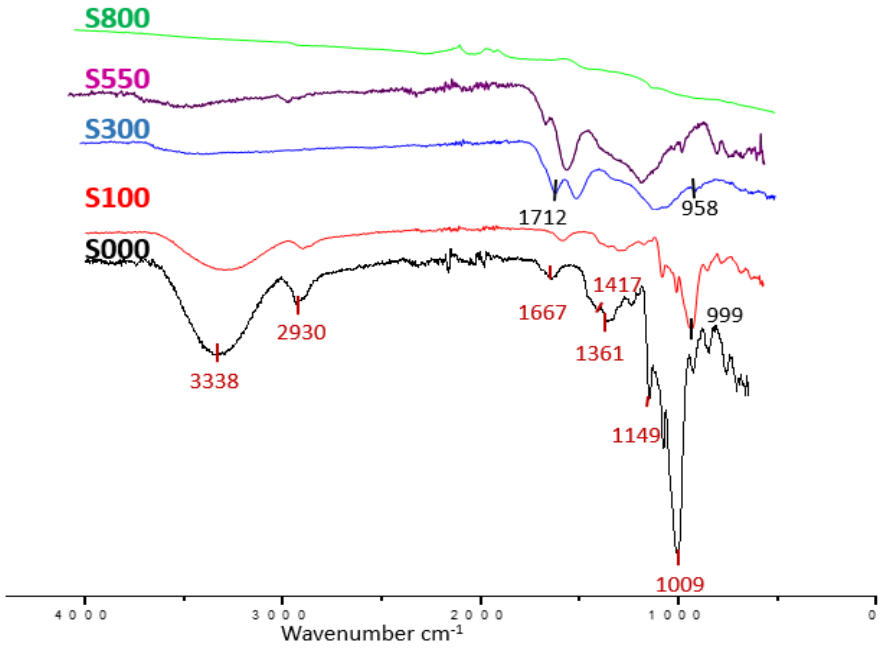

Figure 6. DRIFT-FTIR spectrum of expanded starch and Starbons, obtained at temperatures of 100, 300,550 and 800 ℃

The spectra ATR-FTIR spectra shows the decreasing intensity of the OH stretch at 3300 and 1000 cm^{-1} (labelled in Fig 6) and the increase in graphitic bands as the pyrolysis temperature increases.

Carbonyl groups conjugated with olefinic will form at 958 and 1712 cm^{-1} (Fig 6)[70,71] and vinyl ether groups (large, intense band ranging from 950–1200 $cm^{-1}$with a maximum at 1223 cm^{-1}) take place.

Aromatic bands are added to the spectrum in Fig 7 and shown in S300-550 at 881,825,759 cm^{-1} and at 1599 and ~ 3020 cm^{-1}. S800 is the most graphitic-like and its aromatic C-H have low intensity at 860-680 cm^{-1} and at ~ 3030 cm^{-1}(Fig 7). After S800 the aromatic groups formed previously will condense to graphite-like structures.

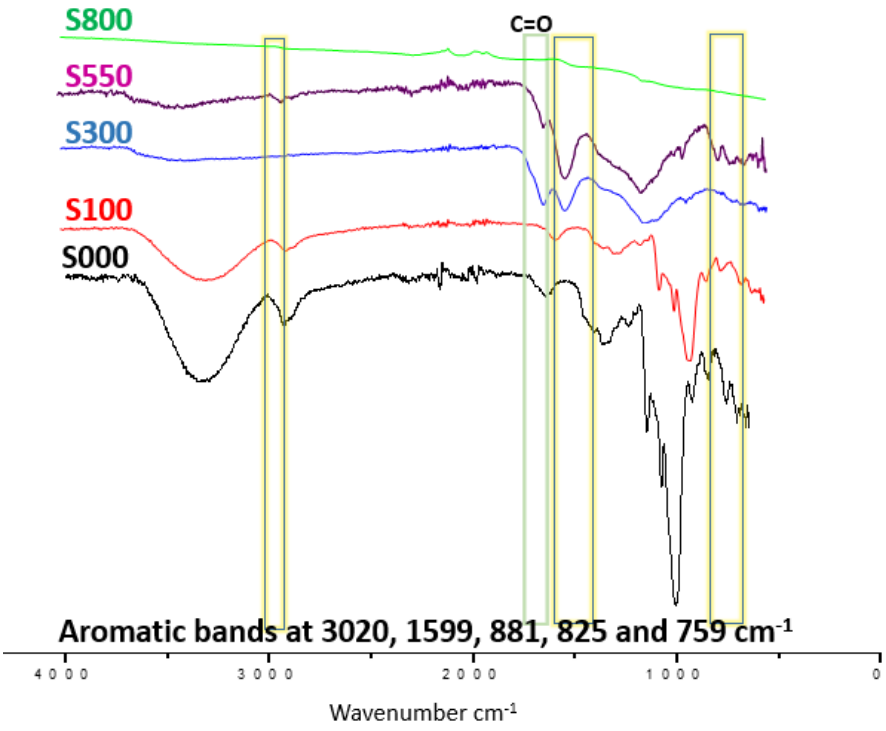

Figure 7. Influence of the Starbon temperature preparation on intensity of aromatic and carbonyl groups adsorption (DRIFT-FTIR results)

The elemental analysis data (Table5 in the Appendices) shows that the carbon content increases with the temperature of Starbon preparation and the hydrogen and the % rest content decreases. For starch derived materials, the carbon content by combustion analysis does not increase further above.

The carbonization trend is reflected in the elemental analysis (CHN) too, the ratios are slightly lower for the bulk (elemental analysis) than for the surface (XPS) of the materials. S300 showed a C:O ratio of 3:3 for CHN analysis and 3:6 for XPS analysis. This suggests that the mechanism of the carbonisation process initiates from the outer surface into the inner bulk of the material.

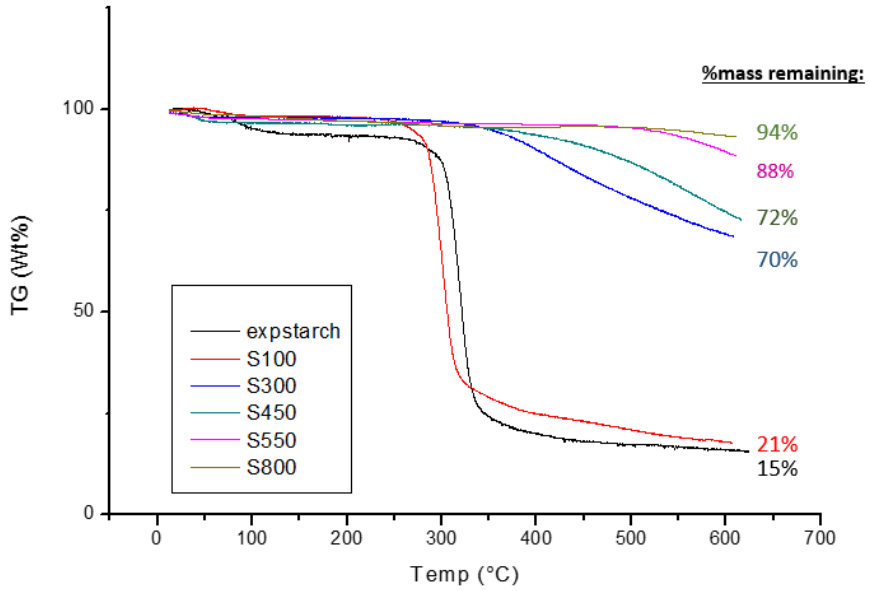

Figure 8. Thermogravimetric analysis of the expanded starch and Starbon obtained at temperatures of 100, 300, 450, 550 and 800℃ and the wt% remaining after carbonisation at 625C

When heated starch demonstrates 85% weight loss and 79% for S100,30% for S300, 28% for S450 ,12% for S550 and only 6% for S800 (Fig 8). The decomposition temperature increases with increasing carbon content, so the low temperature materials decomposed earlier.

2.1.2. Monolithic form of Starbon

The process of ‘’starbonisation’’ begins with the thermal swelling and dissolution of polysaccharide granules at 140˚C in an aqueous solution and shaped in a 10ml syringe tube to take its cylinder shape. Retrogradation happens overnight when an extended 3D network is formed. The next step is to exchange to a lower surface tension solvent as water would destroy the porous structure if dried instantly. The cylinder is drowned carefully in ethanol for solvent exchange few times and acetone will follow. P-TSA is added in acetone and the starch-monolith left in for few days. A white cylinder of 5.5 cm in length and 1.5 cm diameter was obtained after drying as seen in Fig 9:

Figure 9. Image of starch-monolith before carbonisation

The cylinder is then carbonised at different temperatures after a new method. To avoid breaking the monolith during the process the white cylinder has been carbonized in a system like in Fig 10, which controls the heating rate, which was very small at the beginning to avoid the monolith to collapse:

Figure 10. Image of the installation used for monolith synthesis

The sand has protected the Monolith from applying the vacuum too fast and collapsing the monolith and carbonizing it slowly. The fine lines are from the sand (scratches when handling) and from layering the gel into the cylinder shape. The pictures prove that there is no crack and the cylinder is strong.

Monolithic Starbon® can be produced using a similar method to that used above for the production of polysaccharide-derived Starbon®.

A cylindrical monolith of 4.5 cm in length and 1cm diameter was obtained, with channels running along the length of the cylinder (Fig 11) was obtained. The material has no cracks, though foam prints arising from handling it during the solvent exchange and carbonisation process are visible.

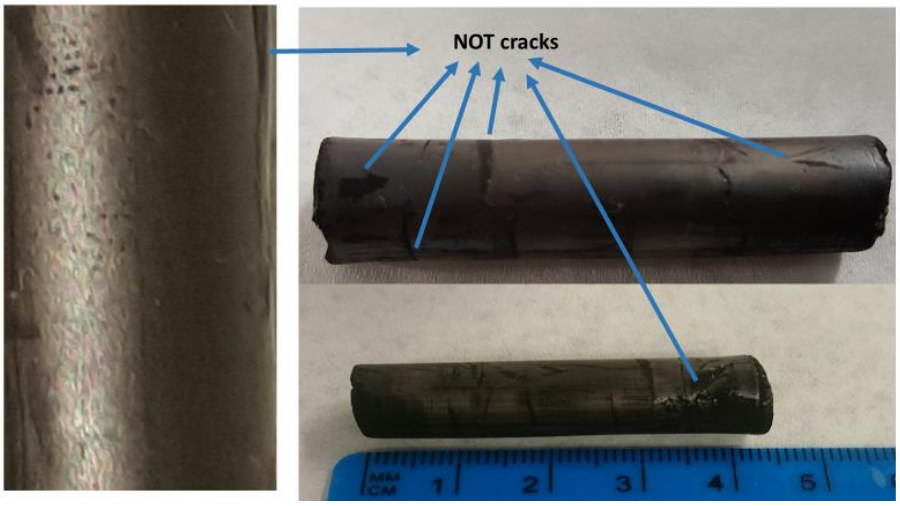

Figure 11. Image of M300 showing no cracks but foam prints

When heated M300 demonstrates 43% weight loss and 21% for M800 (Fig 12).

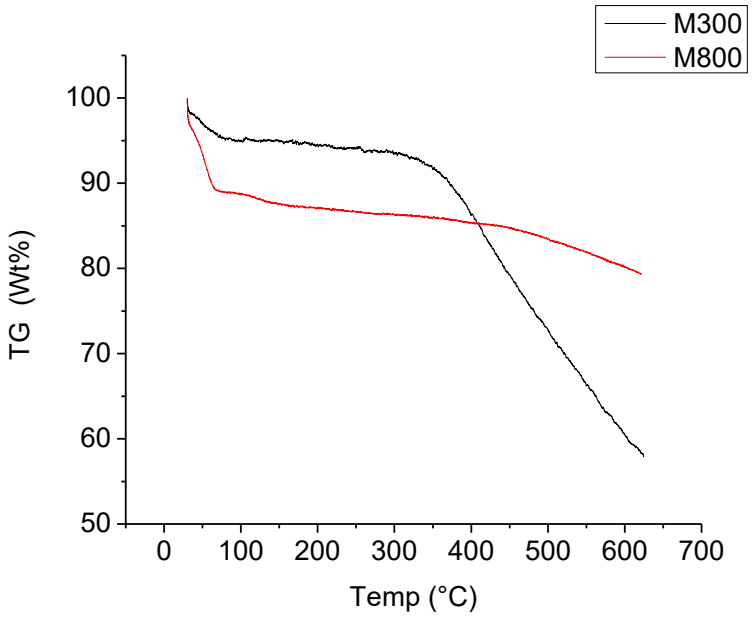

Figure 12. Thermogravimetric analysis of monolith form of Starbon prepared at temperatures of 300 and 800 ℃

The decomposition temperature increases with increasing carbon content, so the low temperature materials decomposed earlier.

2.1.3. Starbon-graphene composites

The starch-graphene material was produced using solvent exchange method and it was summarised in Fig 13: gelation at 140°C (40g of Starch, TBA+ p-TSA addition: starch +TBA (1:3). While the gel is still hot, before retrogradation, desired concentration of graphene is added. Solvent exchange is performed with a lower surface tension solvent (ethanol, acetone) to replace the water from the pores. A minimum quantity of p-TSA in

water or acetone is added to the alcogel and the drying of a polysaccharide alcogel is proceeded in vacuum to form mesoporous aerogel, which is then carbonised to 300-800°C to form mesoporous carbon. As shown in same figure, the graphene is added after the gel is formed to allow a uniform composition between the starch and graphene:

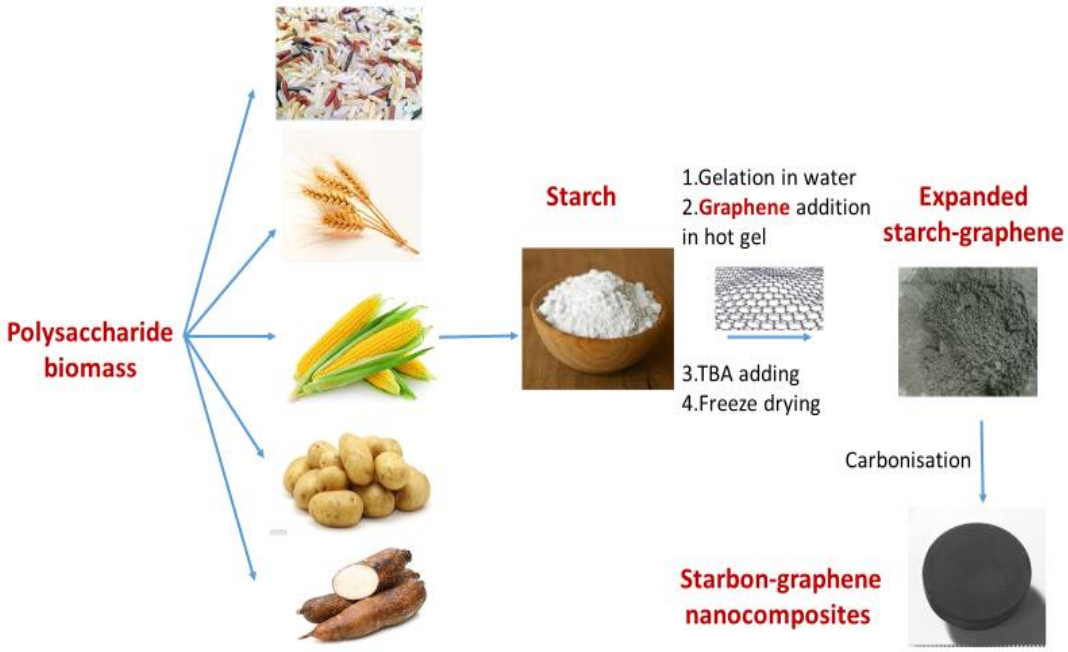

Figure 13. Graphene-derived Starbon synthesis process

The physical properties of Starbon-graphene and pure graphene are listed in Table 2. In the TEM section of the Starbon-graphene nanocomposites it is believed that the light colour is the graphene which is one atomic layer of graphite. Graphite has been easily tested by compressing many layers of graphene together, which is believed to be present in Starbon-graphene material, darker colour of a TEM section of S300 5% graphene (Fig 14, top left):

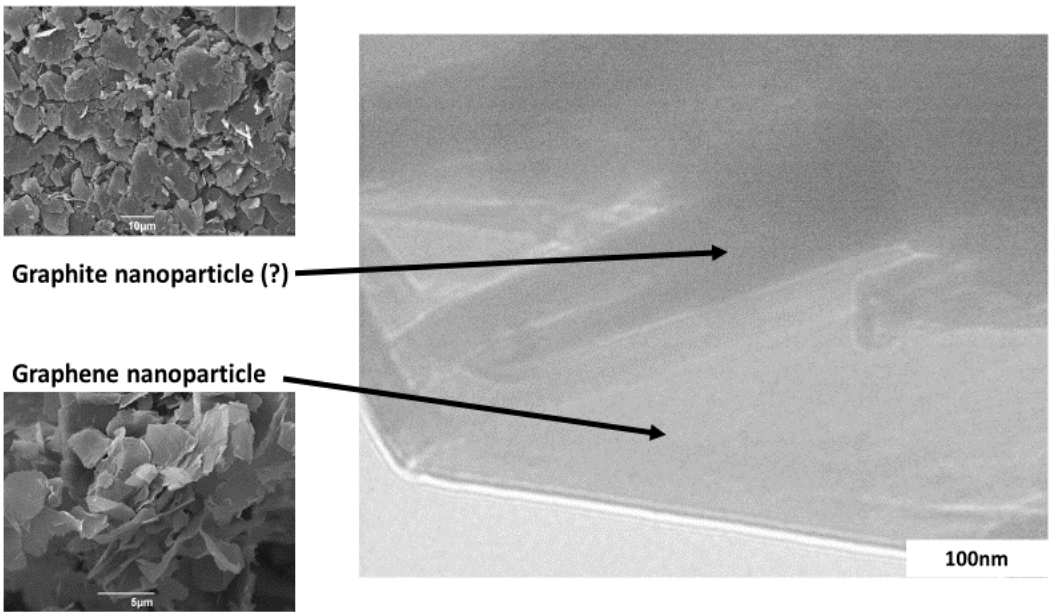

Figure 14. TEM image of Starbon-graphene materials (right) and graphene and possible graphite (left top and bottom)

A SEM section of graphene-derived starbon is shown in Fig 15, where the graphene nanoparticles are visible in big sheets while the Starbon is the porous material:

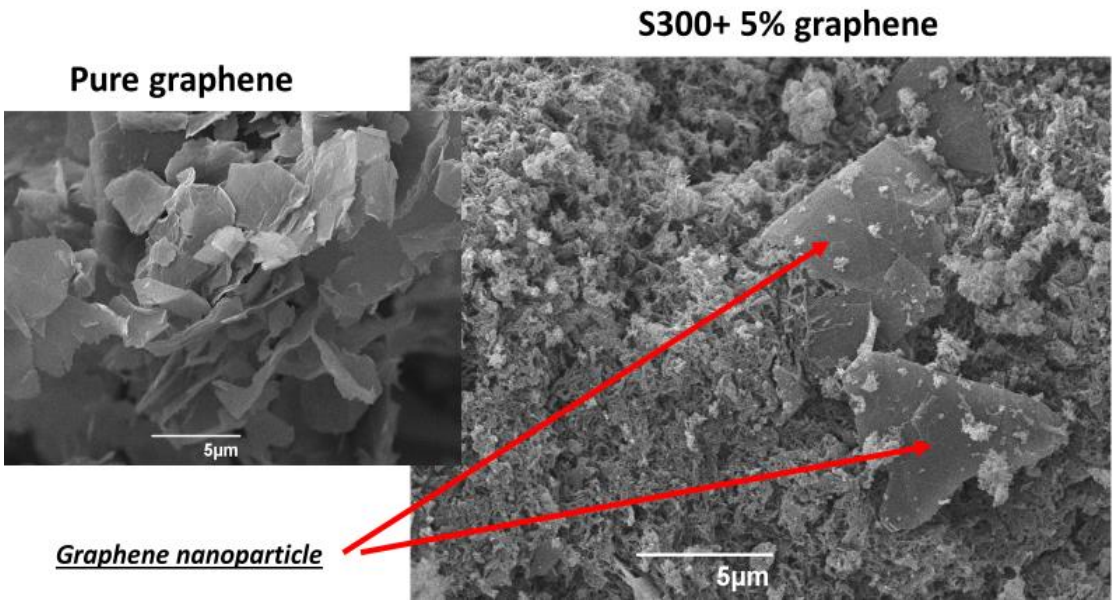

Figure 15. SEM image of Starbon-graphene materials and the presence of the graphene nanoparticles

Graphene has high thermal stability[72] which can be visible through carbonisation, the nanoparticle being present in expanded starch containing 5%graphene starch and also Starbon® with 5%graphene (Fig 16):

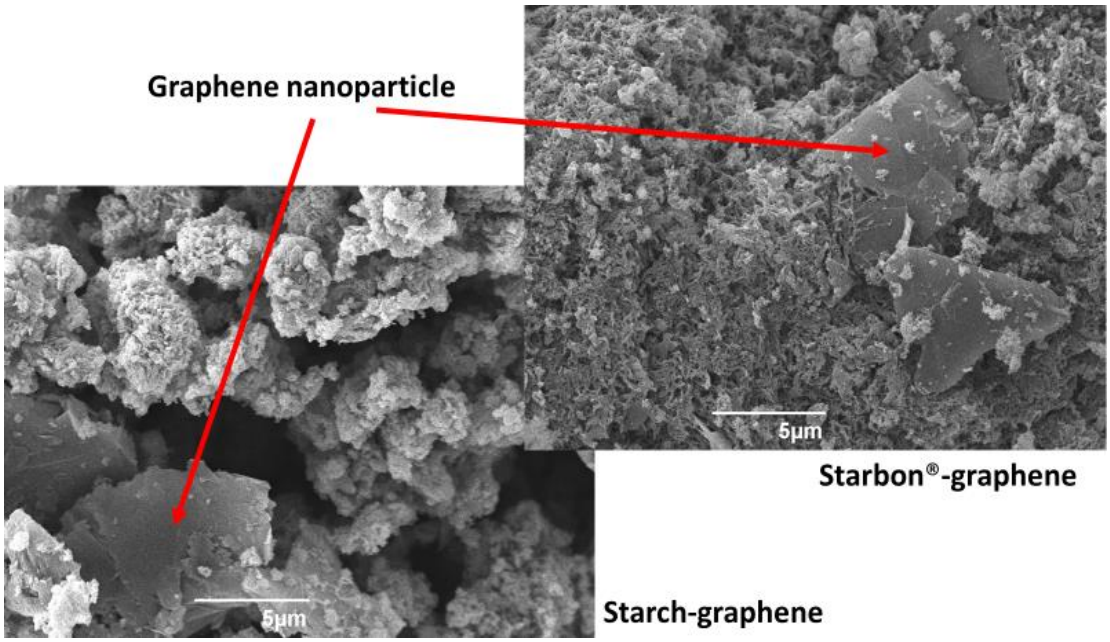

Figure 16. SEM image of dispersion of graphene in the new graphene composites (starch 5%graphene and S300 5%graphene)

When heated S300 with graphene demonstrates 45% weight loss and 20% for S800 with graphene the mass loss being shown in the Fig 17. The decomposition temperature increases with increasing carbon content, so the low temperature materials decomposed earlier.

The new Starbon-graphene has less micropores than unmodified Starbon, but it's more mesoporous (Table 2 and Table 3).

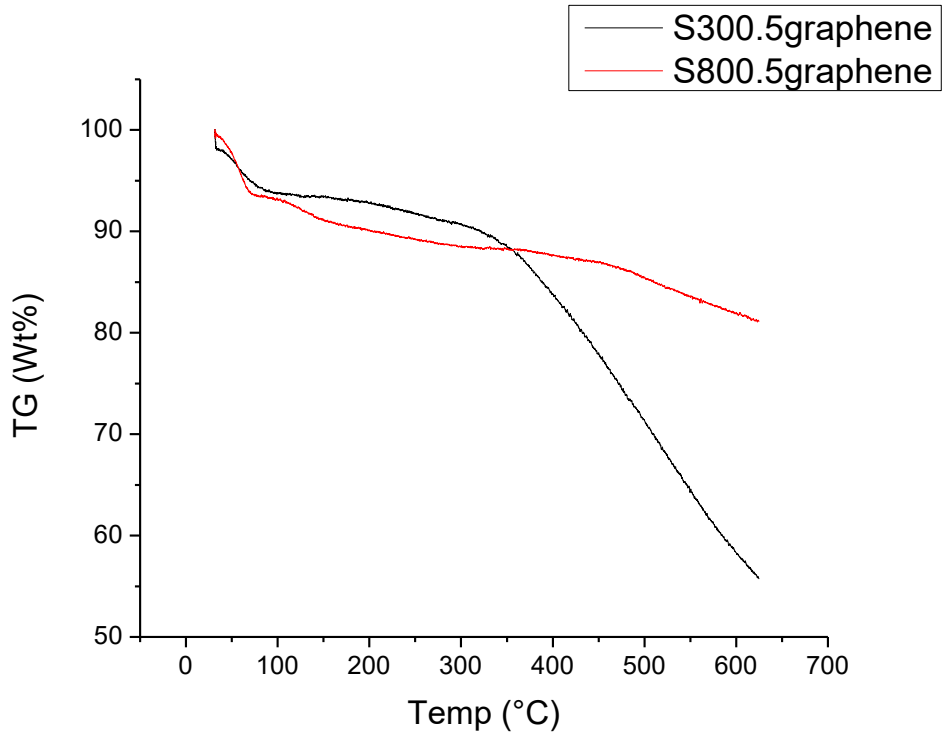

Figure 17. Thermogravimetric analysis of Starbon with 5% graphene obtained at temperatures of 300 and 800C and mass loss when cabonising these materials at 625C

2.2. CO_2 adsorption

2.2.1. CO_2 adsorption on polysaccharide-derived Starbons

To identify the nature of CO_2 adsorption, Starbon® samples was investigated using a Stanton Redcroft STA 625 thermal analyser, in alumina crucibles (sample weight 5-10.0 mg), heated at 1°C min^{-1} to 35°C under flowing N_2 gas (60 mL min^{-1}). Mass of CO_2 adsorbed and heats of adsorption were determined by differential scanning calorimetry (DSC) under atmospheric flow conditions. Before each measurement, all powdered samples were heated at 200°C for 1 h under a flow of N_2 to ensure the removal of residual water and solvents. A three-way valve was employed to switch between feed (CO_2) and inert gas (N_2) for adsorption and desorption measurements. Water adsorption experiments and adsorption isotherms were recorded at 25°C using mixtures of anhydrous N_2 and water saturated N_2.

Rates of adsorption and desorption were calculated after drying the materials, their pressurization and vacuum steps (to remove the CO_2 adsorbed) and used to calculate the mmols of CO_2 adsorbed per gram of sample.

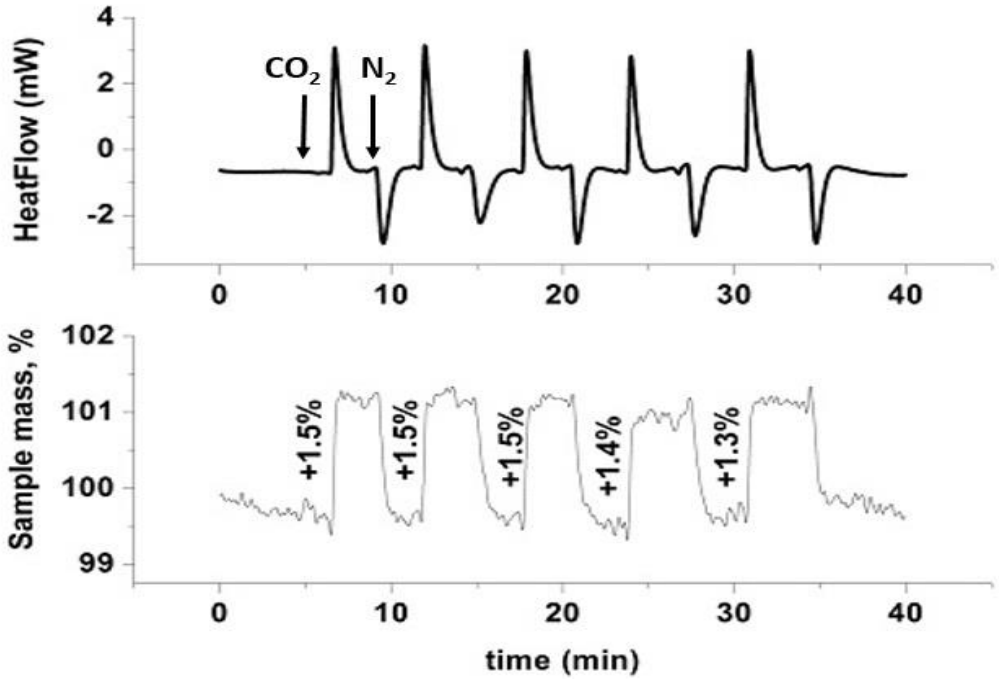

Figure 18. STA plot of mass and heat flow change during six cycles of CO_2 adsorption and desorption using 5.7 mg of AC, at 35 ℃, 100% CO_2/N_2 flow for adsorption/desorption

The mass increases when CO_2 is added and positive heat flows appear like in the example from Fig 18. The mass decreases and negative heat flows coincide with the gas flow being changed back to 100% N_2. This approach shows that the adsorption process on Starbon materials is completely reversibly at constant temperature and pressure. The adsorption was carried out at 35°C and has been influenced by gas concentration, water and time.

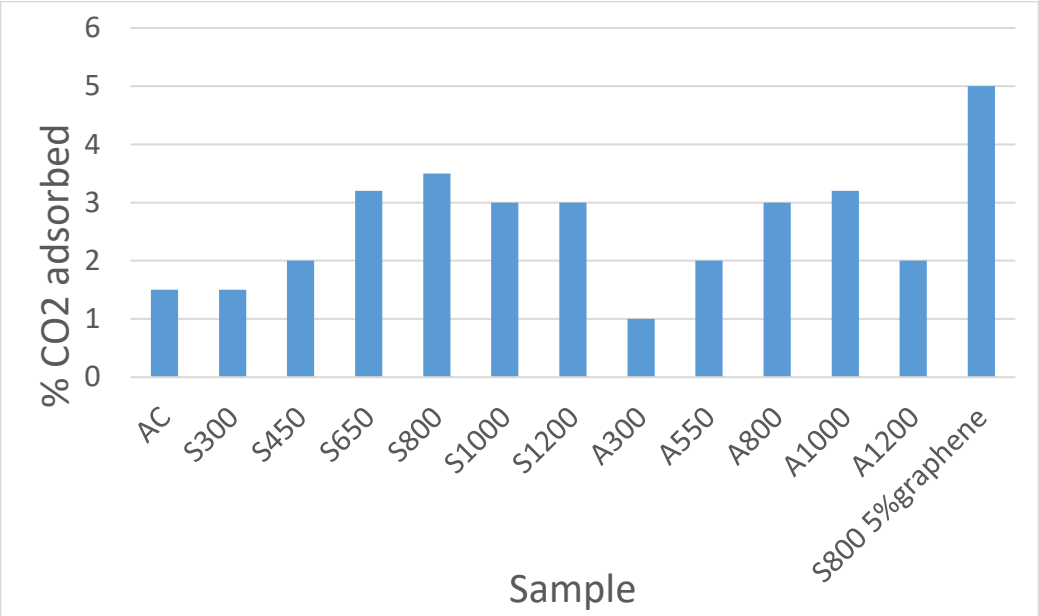

Figure 19. Mass of CO_2 adsorbed onto AC, Starbons and Algibons at different temperatures of cabonisation

The presence of interconnected micropores and mesopores is responsible for the enhanced CO_2 adsorption. Fig 19 shows how the graphene-material adsorbs 75% more CO_2 and starch alginic acid derivatives carbonised above 450°C adsorb more CO_2 than AC. Starbon adsorbs more CO_2 because they these molecules are less restricted and have higher mobility than on AC surface, possibly due to larger micro-/mesopority of Starbon® than AC.[73] For both starch- and alginic acid-derived Starbons® the best results were obtained using high thermal temperatures , these materials having the highest total surface area too, such as S800, S800 5% graphene and A800(Table 1). Starbon-graphene materials adsorb bigger quantity of CO_2 because graphene material has bigger mesoporous volume. Because CO_2 adsorption is mostly reversible,100% of desorption is observed for all samples. In Fig 20 all the materials have CO_2 adsorption enthalpies in the range of -14 to -22 $kJmol^{-1}(CO_2)$. These are in between values of heat of carbon dioxide vaporization (10.3 $kJmol^{-1}$)[74] and sublimation (26.1 $kJmol^{-1}$)[75] and indicate that for all of these materials predominant is the adsorption mechanism:

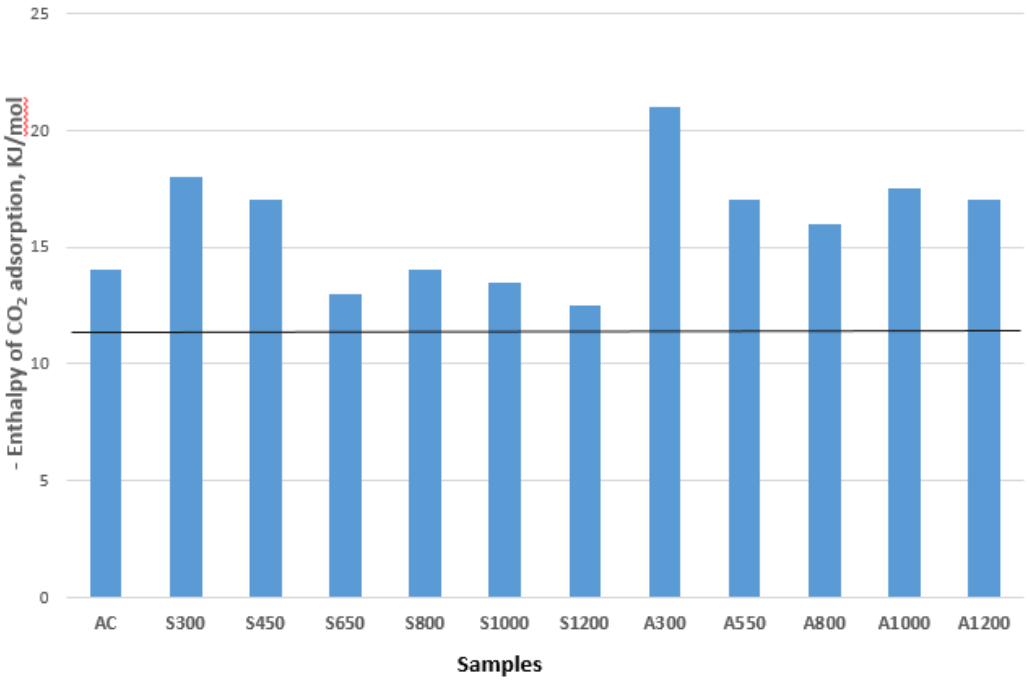

Figure 20. Influence of the Starbon temperature preparation on enthalpies of CO_2 adsorption at temperature of adsorption at 25 ℃

The enthalpy of CO_2 adsorption on the high temperature Starbons® are similar to that of Norit activated carbon suggesting that the adsorption mechanisms are the same and that the role of the mesopores is to make more micropores accessible to CO_2.

The low adsorption enthalpy and the process of physisorption make the process reversible with no large energy requirement, CO_2 capture and release occurring under pressure swing rather than temperature swing conditions.

2.2.1.1. Time influence on CO_2 adsorption

The rate of CO_2 adsorption and desorption is clearly also extremely rapid. It only takes 4 min for S800 to completely saturate with CO_2 before the desorption occurs (Fig 21):

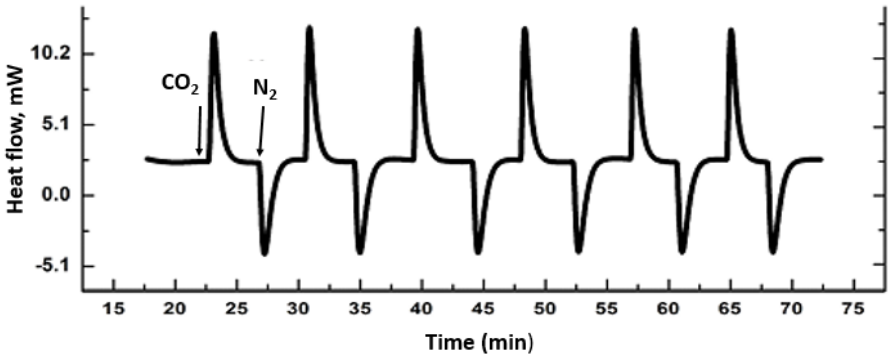

Figure 21. Time influence on reproducibility of the CO_2 adsorption. STA experiment of 9 mg of S800, 35 ℃, 100% CO_2 and N_2 for adsorption/desorption

S300 needs 5 min to adsorb enough CO_2, S450 needs 7 min, S650 6 min, S1000 7 min and S1200 5 minutes. AC needs 4 min for adsorption, A300 needs about 6 min to adsorb CO_2, A800 and A1000 need 5 min and A1200 needs 8 min.

2.2.1.2. Water influence on CO_2 adsorption

Materials carbonised at low temperature (<350^0 C) show similar chemistry to the parent polysaccharide and are relatively hydrophilic, good in applications in aqueous phase[76,77] permitting water adsorption, but molecules as nitrogen shows reverse of the process (Fig 22):

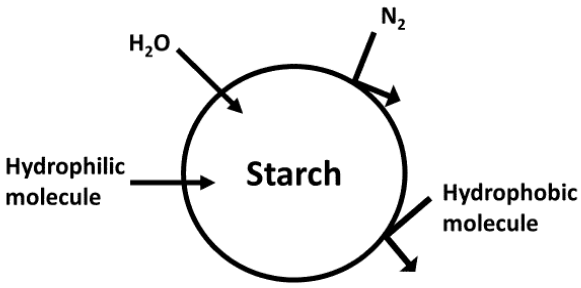

Figure 22. Hydrophilic/hydrophobic character of starch composites

The effect of water on the adsorption of CO_2 was investigated at 25°C by STA using CO_2 which had been pre-saturated with water and a10–20% reduction in the CO2 adsorption capacity of powdered AC, S800, and A800 was observed. The starbon/algibon materials maintained their advantage over AC. Water adsorption isotherms were obtained for AC, S800 and A800 and shown in Fig 23 where starch-derived materials adsorb more than alginic acid derivatives or activated carbon:

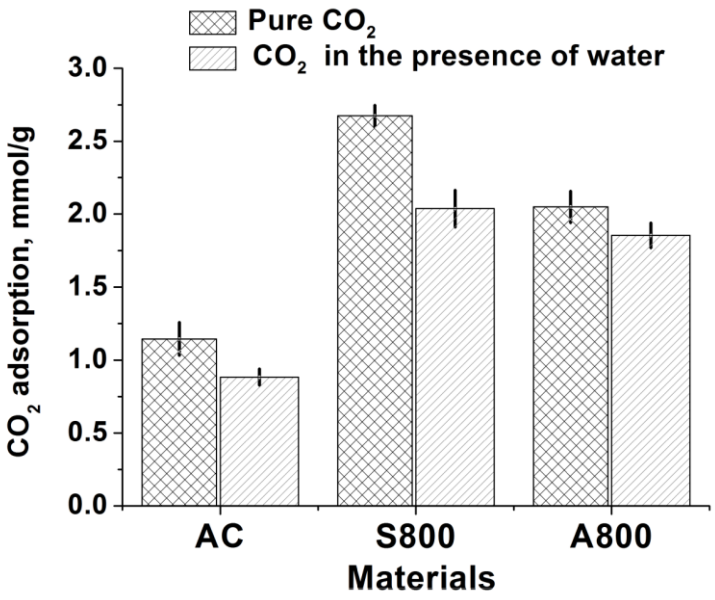

Figure 23. Dry and wet CO_2 adsorption onto activated carbon, starch and alginic acid derivatives

In Fig 24 the low temperature materials will adsorb more water than high temperature materials because of the hydrophilic character of low temperature materials, high temperature ones being hydrophobic:

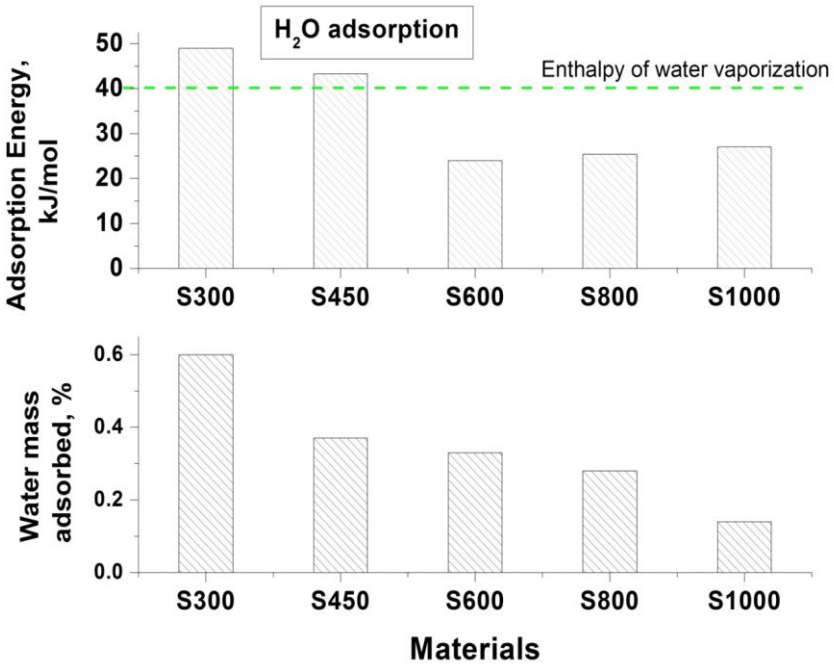

Figure 24. Comparison of water adsorption on Starbons from hydrophilic (S300) to hydrophobic (S800)

The adsorption of water at P/P_0=0.7 was also investigated for the starch derived Starbons and was found to be very low (0.08 mmol H_2Og^{-1} for S1000 to 0.3 for S300 mmol H_2O g^{-1}).

2.2.1.3 CO_2/N_2 mixtures influence

CO_2 adsorption process on Starbon materials is completely reversibly at constant temperature (35°C) and pressure as the composition of CO_2/N_2 ratio changes.

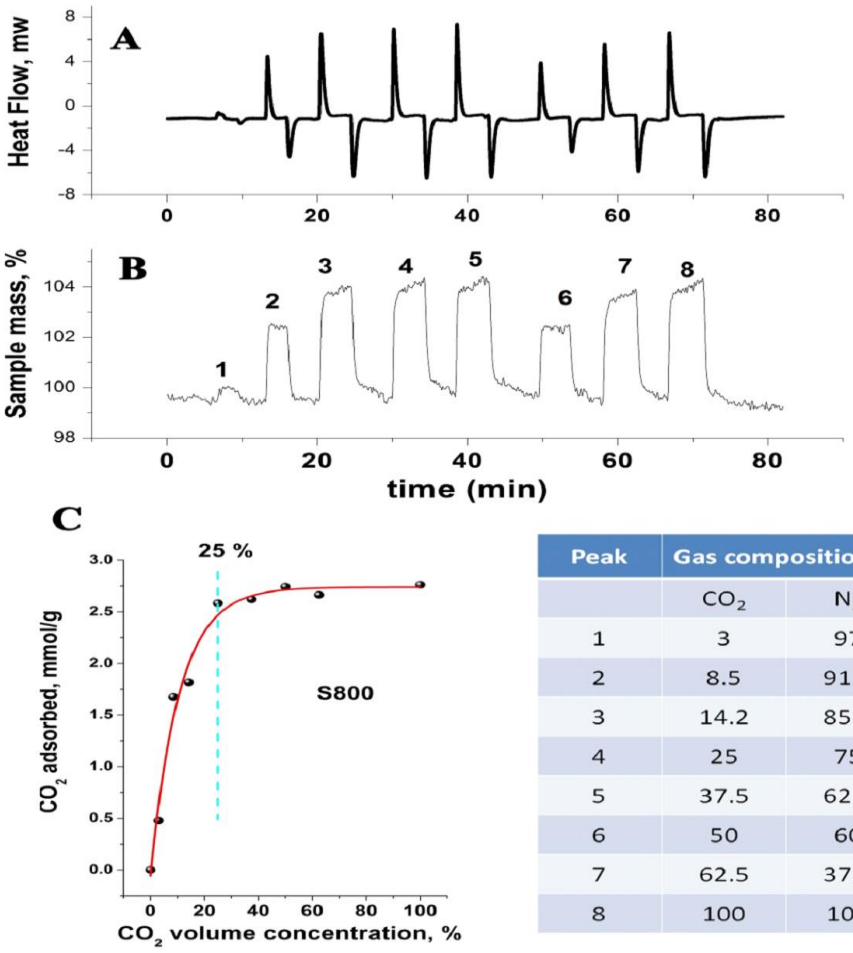

Peak	Gas composition %	
	CO_2	N_2
1	3	97
2	8.5	91.5
3	14.2	85.5
4	25	75
5	37.5	62.5
6	50	60
7	62.5	37.5
8	100	100

Figure 25. Adsorption and desorption using different ratios CO_2/N_2

In CO_2/N_2 mixtures S800 and A800 need at least 25% gas in nitrogen to reach the concentration of CO_2 as it was adsorbed at 100% (Fig 25). AC needs at least 50% to have the same CO_2 volume concentration.

2.2.2. CO_2 adsorption on Starbon-graphene composites

S800 5% graphene showed bigger adsorption performance of CO_2 because the Graphene material has bigger mesoporous volume.

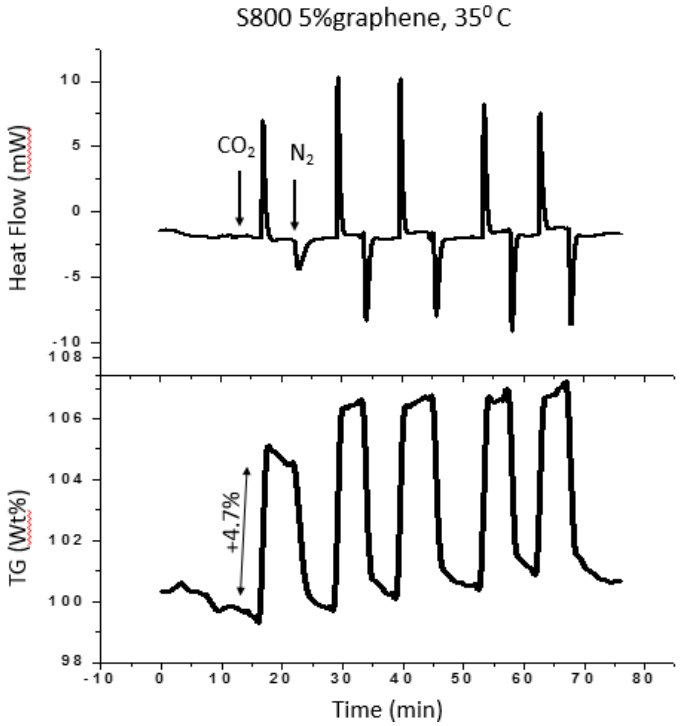

Figure 26. Mass and heat flow change during CO_2 adsorption and desorption using S800 5% graphene at 35 ℃

As S800 5%graphene developed a high adsorption performance (Fig 26) it's expected that all graphene-starbons to develop higher adsorption than their polysaccharide-derived Starbons, but lower than S800 5%graphene.

2.3. NH_3 adsorption

2.3.1. NH_3 adsorption on polysaccharide-derived Starbons

2.3.1.1. Surface chemistry influence

STA plots of mass and heat flow change during cycles of NH_3 adsorption and desorption using S300 at 35°C is shown in Fig 24. Ammonia gas diluted in N_2 flow was introduced using a 50ml syringe, at 2ml/min flow at 35° C. During the desorption stage ammonia flow was stopped and nitrogen was introduced.

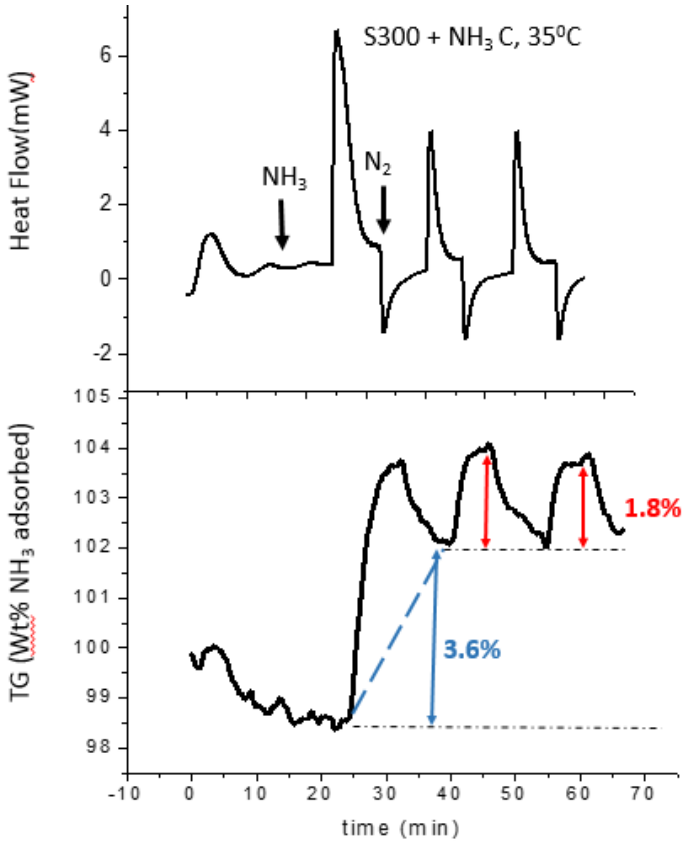

Figure 27. Mass and heat flow change during NH_3 adsorption and desorption onto S300 at 35 ℃

Starbon developed surface functionalities tuneable between hydrophilic to hydrophobic[78] during carbonisation and this is observable during ammonia adsorption. In Fig 28 as long in S800 only occurs physisorption, a fast process with reversible desorption, in S300 chemisorption occurs. Chemisorption, which is irreversible under these conditions, occurs as the first stage of adsorption, until certain pores are filled and then reversible physisorption is observed as a second stage.

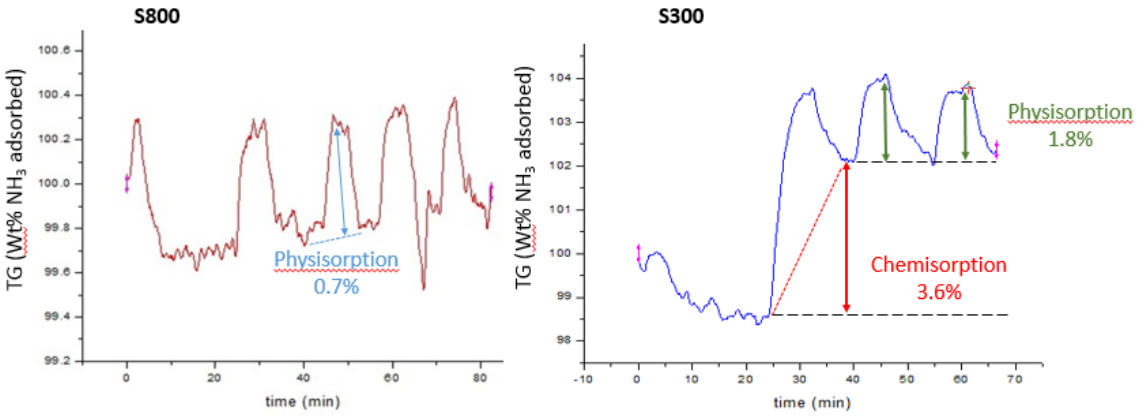

Figure 28. Comparison of physi/chemisorption onto S800 and S300

Fig 29 shows how physisorption is possible due to macro and micro-/mesopores, chemisorption occurring because of their surface chemistry surface. Starbons carbonised at lower temperature than 450˚C develop chemisorption, this is believed to be a result of the acidic surface reacting with ammonia, a weak base, and form unexpected nitriles, process described later (see ‘’2.2. Synthesis of nitrogen-doped materials’’).

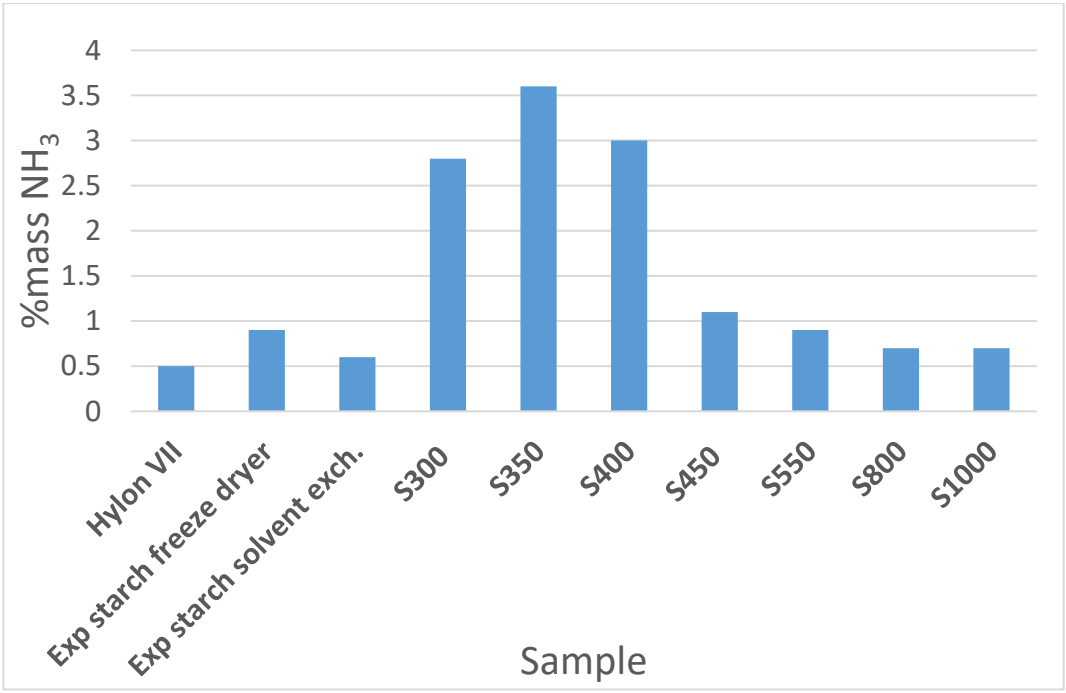

Figure 29. Ammonia adsorption onto expanded starch derivatives

Ammonia is absorbed onto hydrophilic surface, S350 having the biggest performance developing chemisorption when certain pores block and physisorption occurs. After 450ºC micro and micro/mesopores are responsible for physisorption. S800 has the smallest ammonia adsorption performance, smaller than S1000 due to larger micro/mesopore volume of S1000 (with slightly smaller micropore volume) (Table1 in the appendices).

In the alginic acid composites range A350 has the biggest ammonia adsorption, shown in Fig 30, together with expanded alginic acid, but A800 has the smallest capacity of

adsorbing ammonia. However, AC has proven very low ammonia adsorbance performance, even smaller than A800.

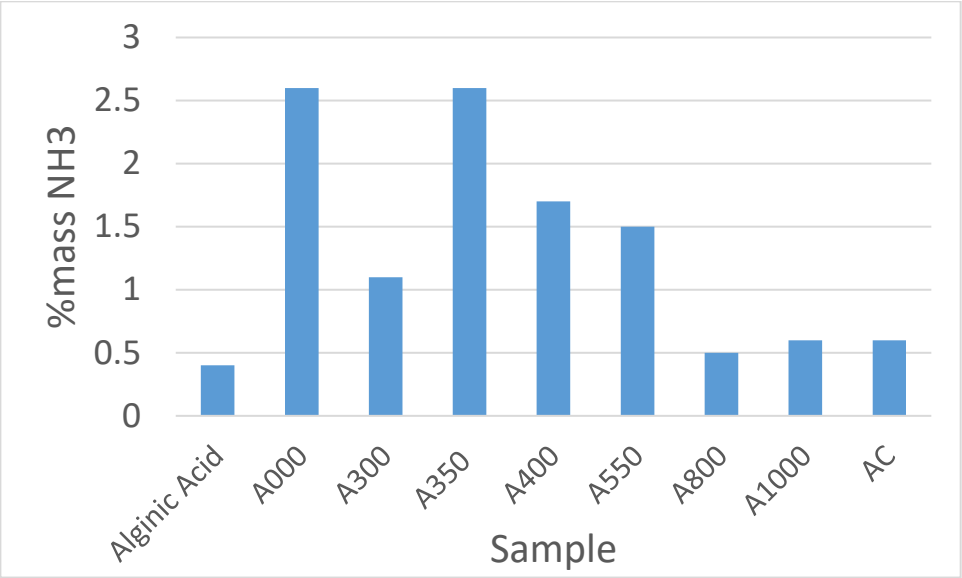

Figure 30. NH3 adsorption onto activated carbon and alginic acid derivatives

S300 absorbs more NH_3 than A300 due to physisorption which occurs in micropores (Fig 31). S300 adsorbs better because the ammonia interacts with the OH groups on the Starbon's surface leading to amines.

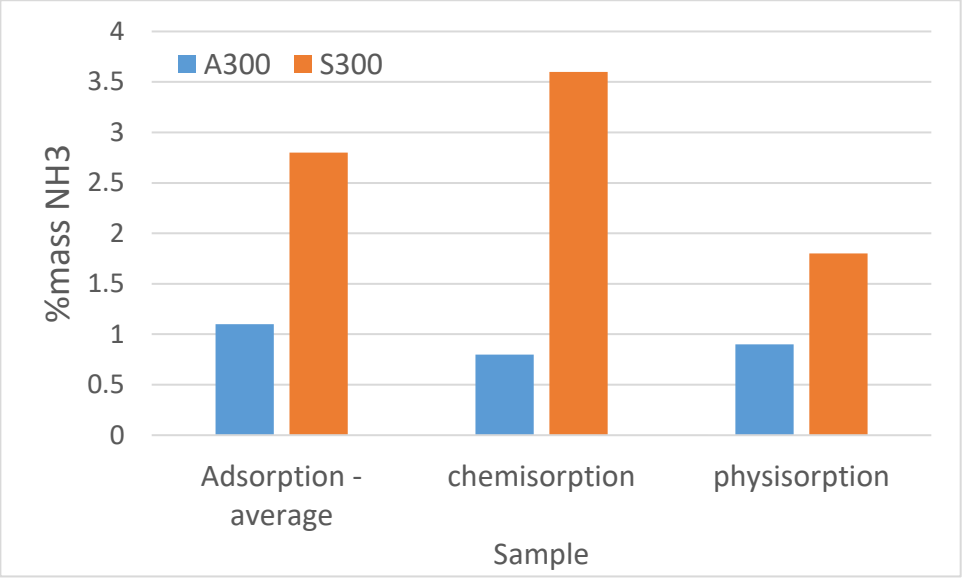

Figure 31. Ammonia adsorption onto A300 and S300, difference in chemi- and physisorption

It has been shown that S350 adsorbs better than S300 because of different chemistry surface between the two materials. Fig 32 shows that S350 has higher intensity at 1718 cm^{-1}(carbonyl group) and vinyl ether groups (1232 cm^{-1}):

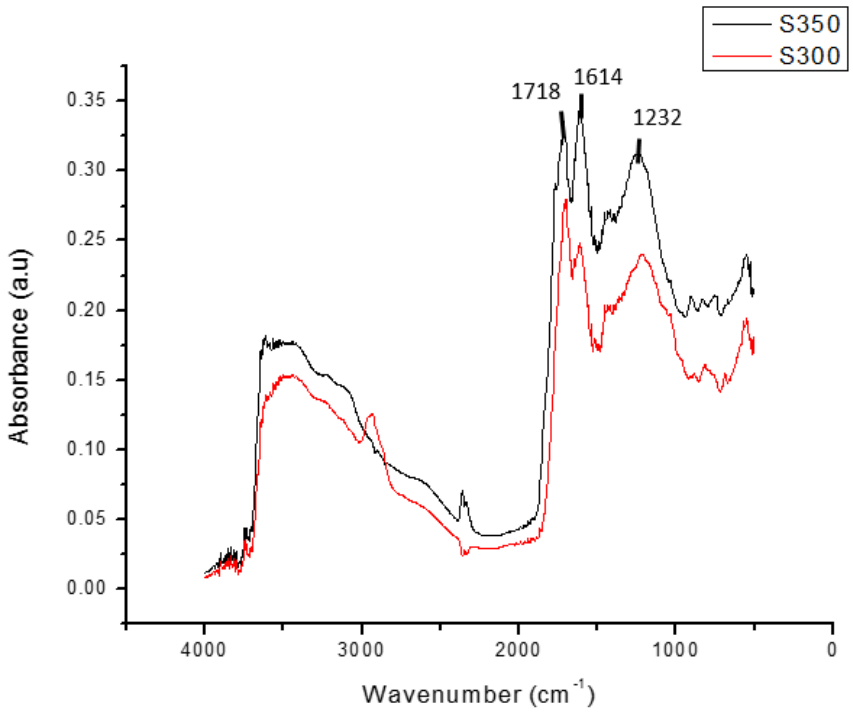

Figure 32. Comparison of DRIFT-FTIR spectra of S300 and S350

Thus more research is required, probably S350 adsorbs better because of bigger concentration of carbonyl groups.

2.3.1.2. Time influence

Physisorption is a fast process and reversible and it's directly proportional with the quantity of ammonia adsorbed and physical properties of the material. S800 has bigger surface area and more micropores than A800, but less mesopores, hence the bigger physisorption.

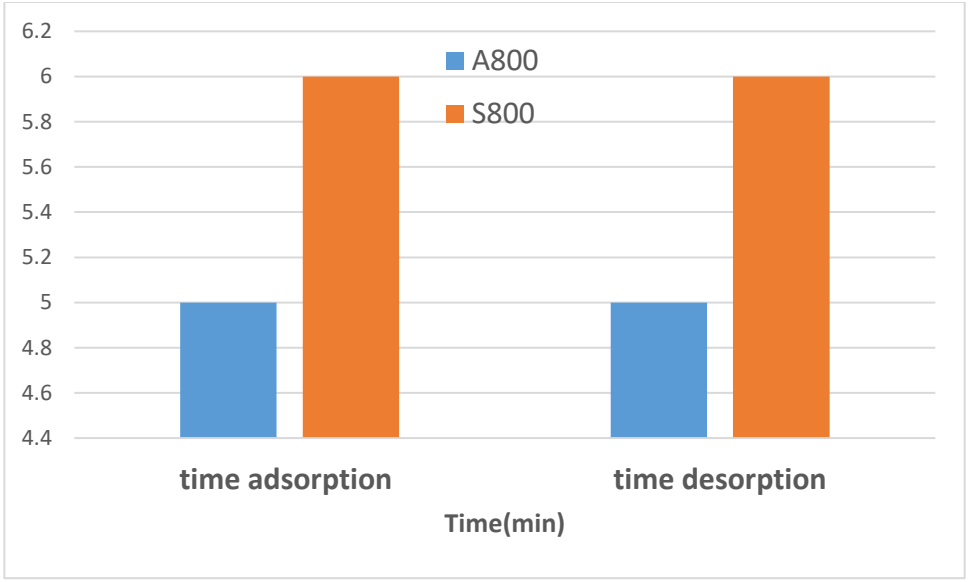

Figure 33. Time influence on physisorption onto A800 and S800

Chemisorption is an irreversible and longer process, directly proportional with the quantity of ammonia absorbed and performance of material's adsorption performance.

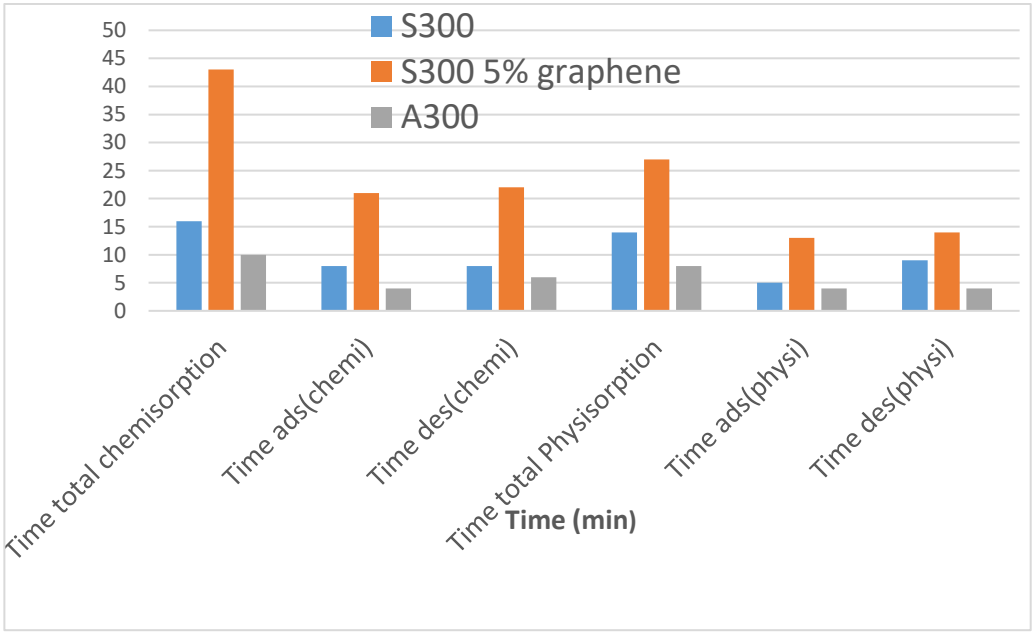

Figure 34. Time influence on chemisorption onto S300, S300 5% graphene and A300

In Fig 34, S300 absorbs more ammonia than S300 5%graphene because of the solvent exchange method of preparation of graphene material, making its physical properties slightly higher and so, more concentrated in acidic surface of S300 than graphene material. However, S300 5% graphene material takes longer to chemisorb probably because of the extra graphene in its composition, making it harder to enter the material's pores. Ammonia will react eventually with the acidic surface of Starbon®. Physisorption is longer too, considering the gas left after the chemisorption needs time to desorb from the pores. The desorption of a chemical process is longer than desorption of a physical process.

2.3.1.3. Temperature influence

Upon increasing the temperature of the ammonia absorption experiment from 35°C to 50°C and then 70°C a slight decrease in the amount of ammonia adsorbed is observed, however, this is comparatively minor (2.5% +/-0.1% in all cases) (Fig 35):

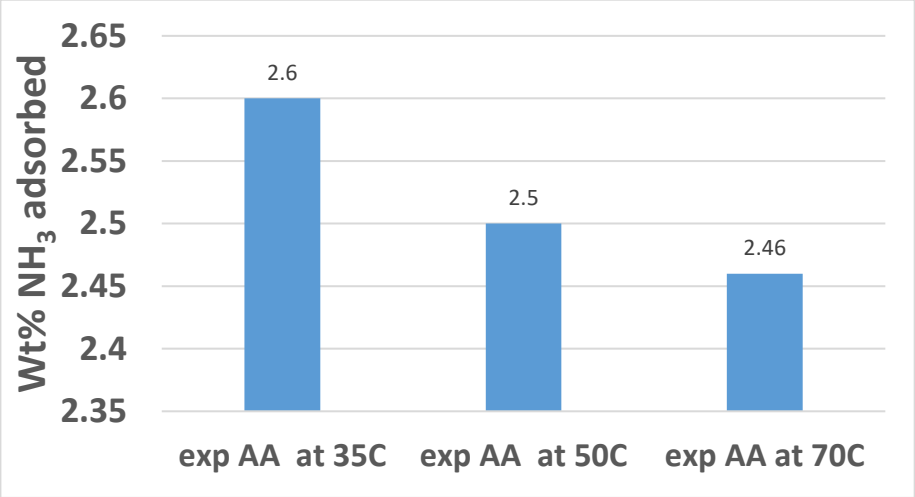

Figure 35. Influence of temperature on ammonia adsorption in the low temperature regime (35, 50 and 70C)

The XPS spectrum of Exp AA+NH_3 (Fig 36) showed 4 peaks in the C1s region; 285.03 eV (sp^2), 283.36 eV, 286.44 eV, and 287.68(nitrile) eV. The N1s region showed 2 peaks; 397.67 eV (pyridinic, imines), 399.57 eV (amines):

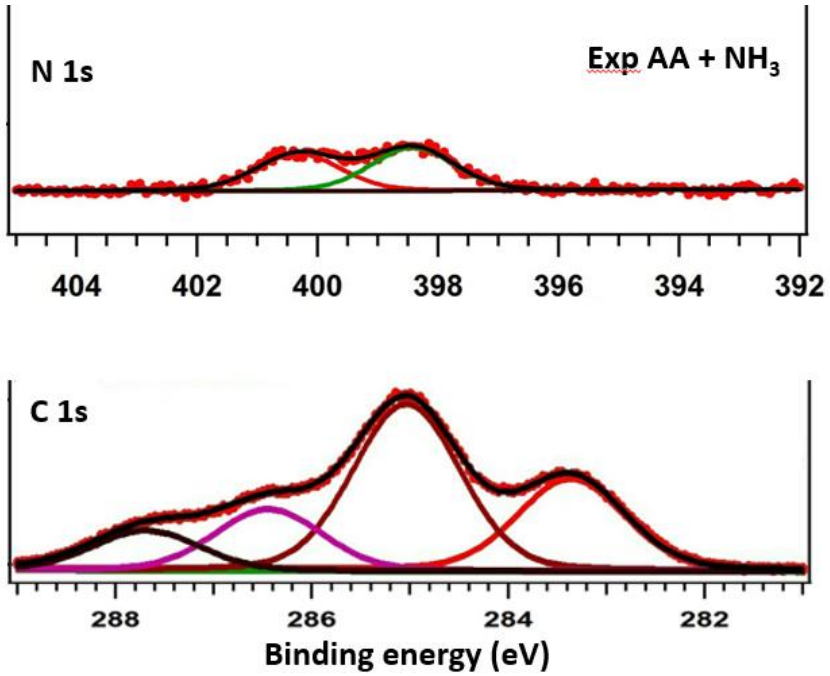

Figure 36. XPS analysis of the expanded starch after ammonia adsorption

Elemental analysis found the nitrogen content to be 4.9 % (C/N ratio of 7.2:1) while XPS found 1.6 % (C/N ratio of 36.9:1), indicated that carbonisation may be inducing loss of nitrogen on the surface but not within the core of material.

2.3.1.4. Method of Starbon synthesis influence

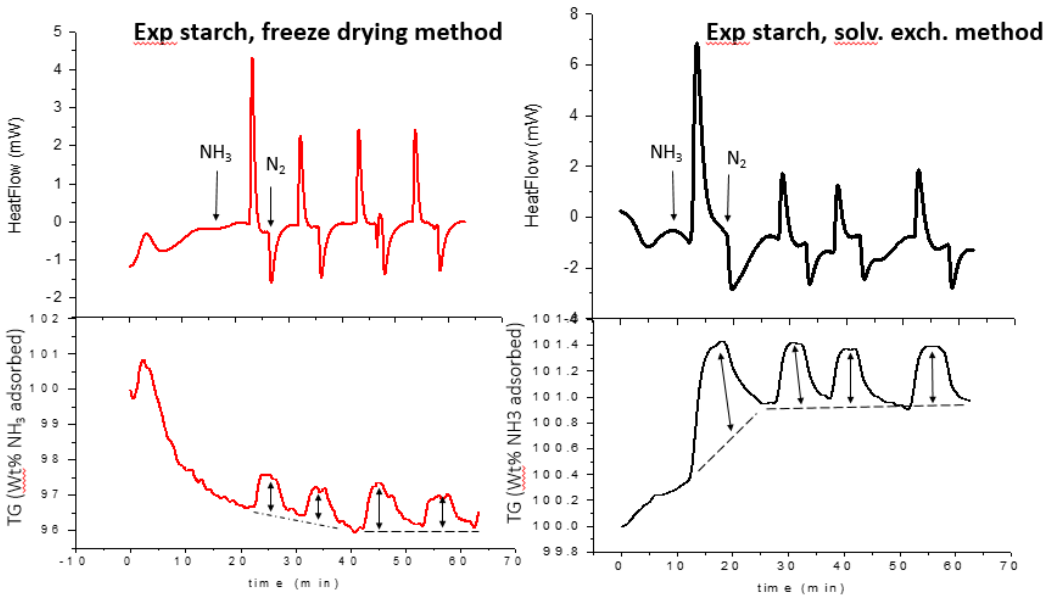

Figure 37. Mass and heat flow change during ammonia adsorption and desorption onto expanded starch (freeze drying and solvent exchange methods), at 35 ℃

The expanded starch obtained with solvent exchange has no micropores and twice less mesopores and lower surface area (Table 3) and it has shown 0.6% of NH_3 adsorption instead of 0.9% for freeze drying method starch (Fig 38). Adsorption and desorption occur faster in freeze dryer method with aprox 4 min/ads and 5min/des. For solvent exchange obtained expanded starch it takes 5 min to adsorb and 6 min to completely desorb.

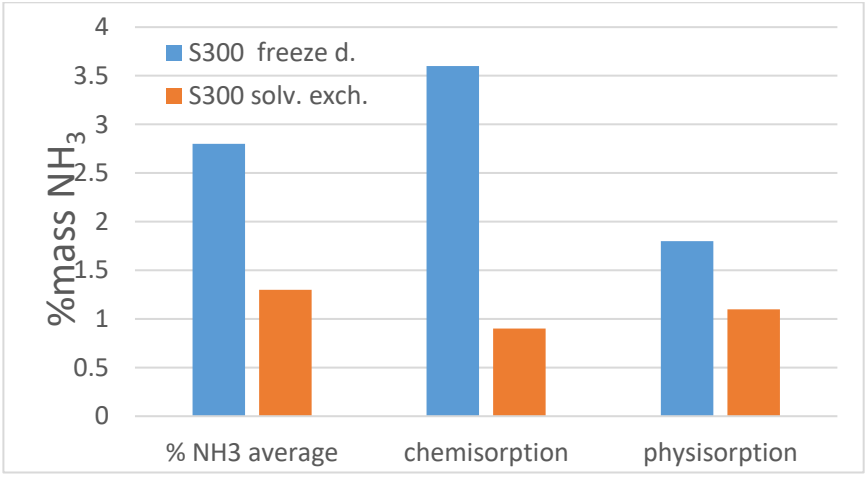

Figure 38. NH_3 adsorption onto S300 prepared with 2 different methods (freeze drying and solvent exchange

2.3.2. NH_3 adsorption on monolithic form of Starbon

It is interesting how the monolithic form of Starbon® interacts with ammonia. The experimental data showed that the adsorption is every time different, depending on monolith part.

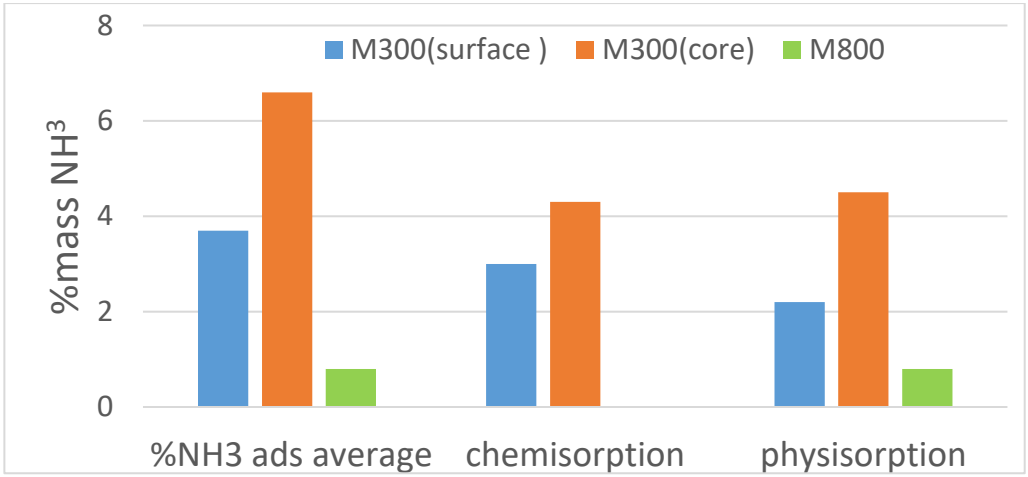

Figure 39. Ammonia adsorption onto monolith form of Starbon carbonised at 300(different parts) and 800C

The process is longer than any other of the Starbon® form because of the compact form of a monolith, 100ml of NH_3 were necessary to perform 2 cycles of adsorption (a chemisorption followed by a physisorption), showing a very long process of ammonia adsorbtion. In Fig 40 it is shown how the core of a monolith adsorbs more ammonia than the edge of it, because the core is more porous than the edge, more information about it following in Fig 41.

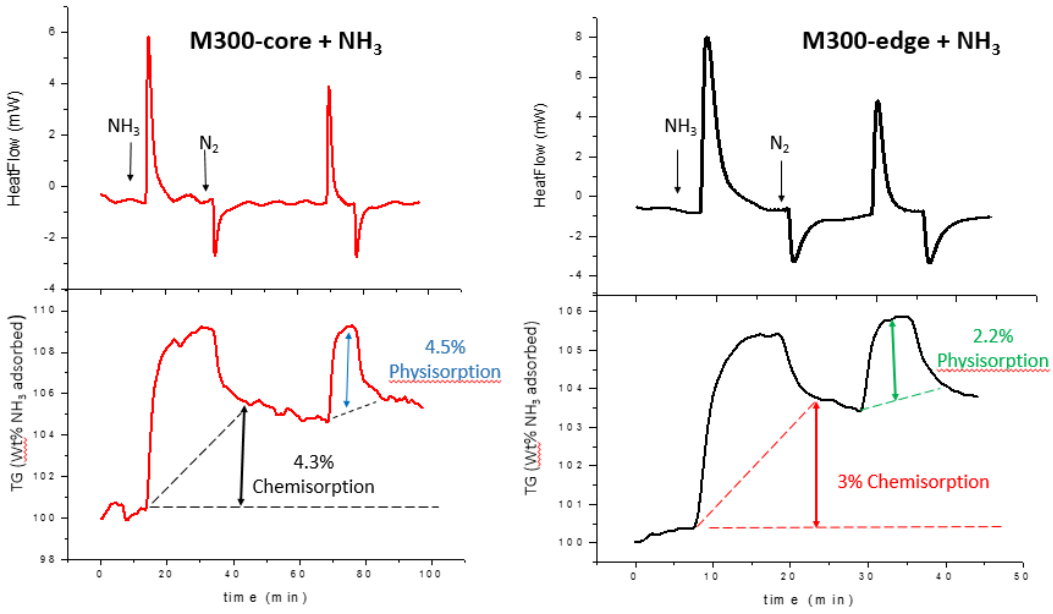

Figure 40. Mass and flow change during adsorption and desorption on M300 (different parts)

M800 only develops psysisorption, but for M300 chemisorption is followed by physisorption (Fig 41). It took only 26 min for physisorption (approx. 8 min/adsorption and 18 min/desorption), but approx. one hour for chemisorption (20 min/adsorption and 35 min/desorption).

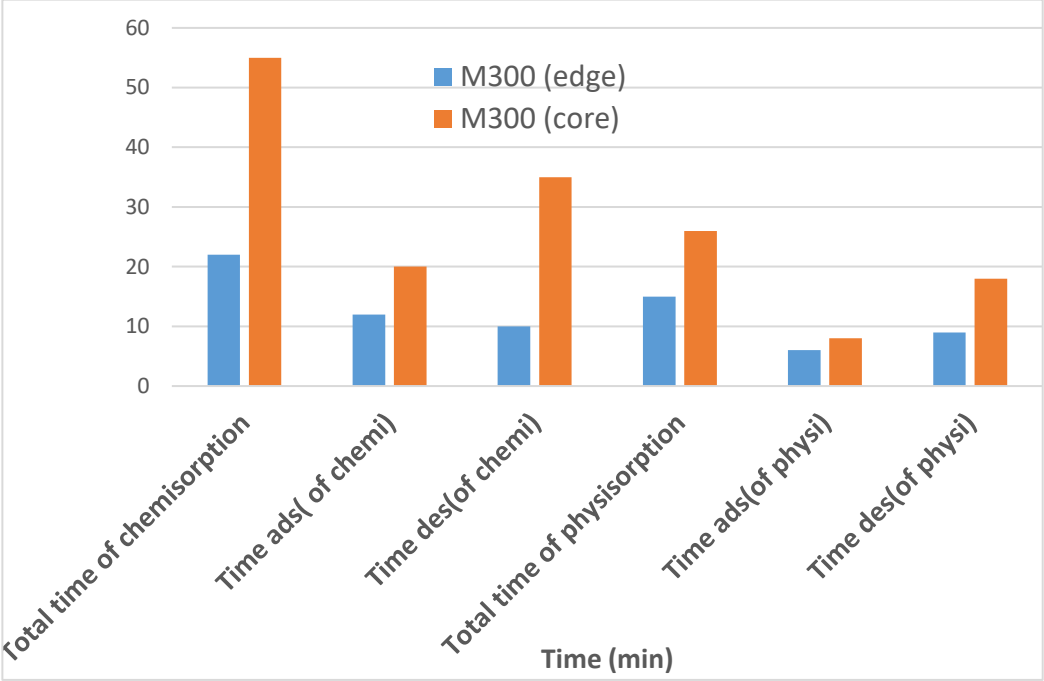

Figure 41. Time influence on adsorption onto monolith form of Starbon (M300 edge and core)

More analyses on monolith form of Starbon represent future work, to check the chemical nature of the new material obtained after absorption of ammonia on it. The bigger quantity of ammonia absorbed, the bigger time of chemisorption is observed on this form of Starbon®. The physisorption takes longer time than any of the Starbon® form because of its structure, entering the monolith pores it's more difficult and so it needs more time than a powder. The ''core'' needs longer time because the shiny part of the ''edge'' is skipped, no adsorption is believed to take place. More analysis like microscope analysis, would probably resolve this uncertain part.

2.3.3. NH_3 adsorption on Starbon-graphene composites

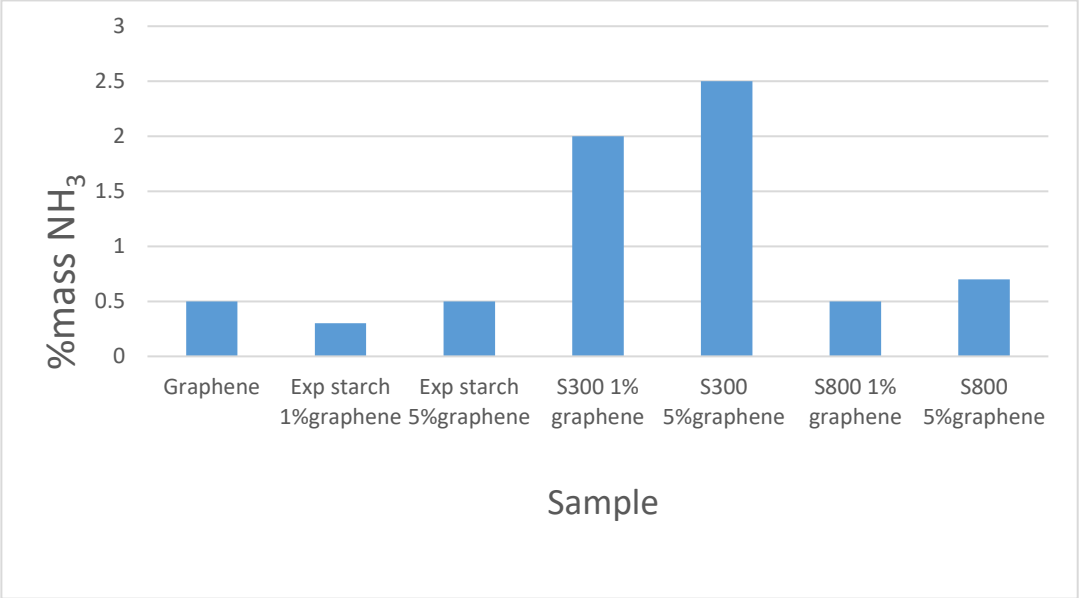

Figure 42. Ammonia adsorption onto graphene composites

Considering the method of synthesis is the same for all graphene composites, the more graphene is added the bigger adsorption. This phenomenon is illustrated in Fig 42 where S300 with 5% graphene performs the highest adsorption of ammonia. Thus starch-graphene are made using solvent-exchange method, these composite would have better physical properties if prepared by freeze-drying method and so, better adsorption performances. However, graphene itself was considered for ammonia (Fig 43) adsorption even if it was difficult to work with the fluffy and very light material, without squashing it to graphite-like structure. Graphene, graphene-starch and S800-graphene developed physisorption, while S300-graphene develop chemisorption first, considering the chemistry surface of starch-derived S300, followed by physisorption.

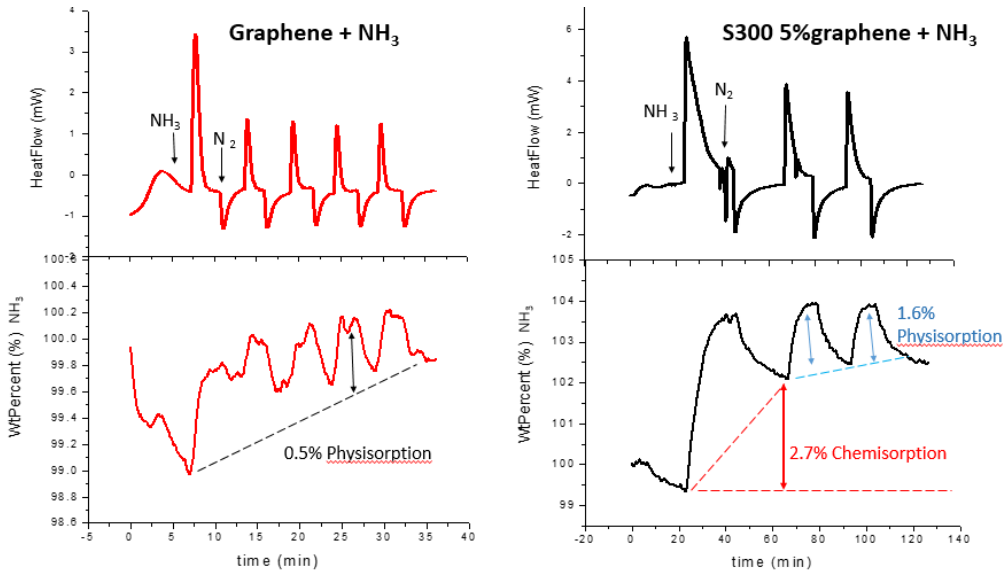

Figure 43. Mass and heat flow change during NH_3 adsorption and desorption using graphene and S300 5% graphene

The physisorption process of graphene is given by its surface area (Fig 44):

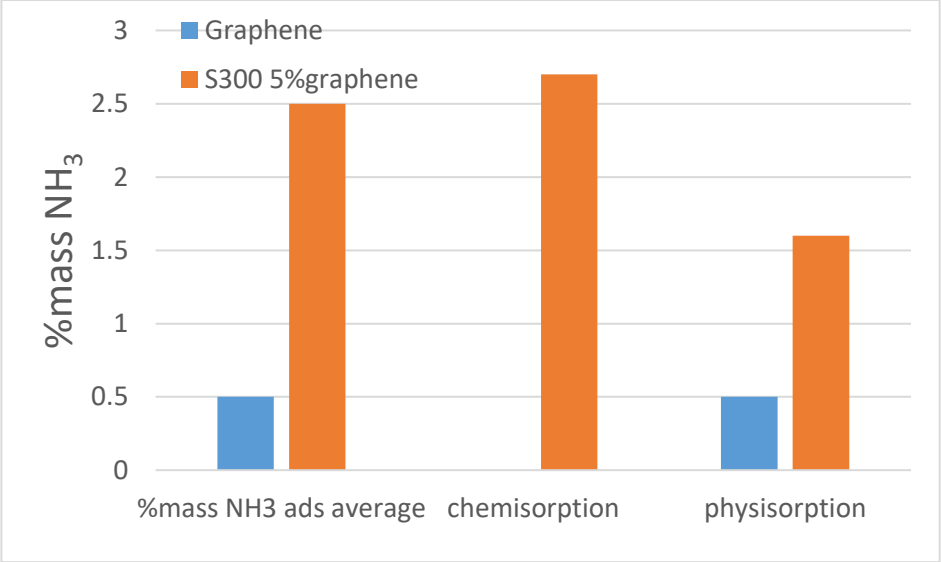

Figure 44. Physi/chemisorption onto graphene and S300 5% graphene

2.4. Synthesis of n-doped materials

During the NH_3 adsorption, Starbons® led to new bio-based nitrile-containing mesoporous materials.
The introduction of nitrogen is expected to improve CO_2 capture performance, heavy-metal binding, conductivity and catalytic activity, most notably in the metal-free oxidative reduction reaction.[79,80,81,82]
Ammonia substitutes hydroxyl groups to form amide, amines, imides, imines, and nitriles dominated at low temperature (bellow 600°C) and thermally stable aromatic rings at higher temperature (>600°C).

A previous study on adsorption of ammonia onto activated carbon[83] describes a possible mechanism for nitrile formation whereby ammonium salts form with carboxylate groups on the surface of the carbon. This is then thermally dehydrated to an amide, and again to a nitrile.

Ammonia may also substitute hydroxyl groups to form amines. Pyridinic nitrogen forms if oxygen in ethers is substituted by – NH –.[84]
The catalytic activity of activated carbons in oxidation reactions with O_2 is increased after treatment of activated carbon with NH_3 or HCN at high temperatures (600-900°C)[16], when the nitrogen content was higher on the surface than in the bulk, but the accessible micropore volume was reduced. When heated up to 900°C, the micropore volume increased, but N_2 volume reduced.

When heating up in ammonia, a high temperature is considered, but it is important to be porous, for a future CO_2 adsorption.

2.4.1. Methods of synthesis of new n-doped materials

2 methods of synthesis of these new n-doped materials were developed (nicknaming them ‘’RBF’’ and ‘’STA method’’):

- RBF method: 100 mg of S300 is heated up to 300°C in a round bottom flask with 257ml NH_3 (Fig 45):

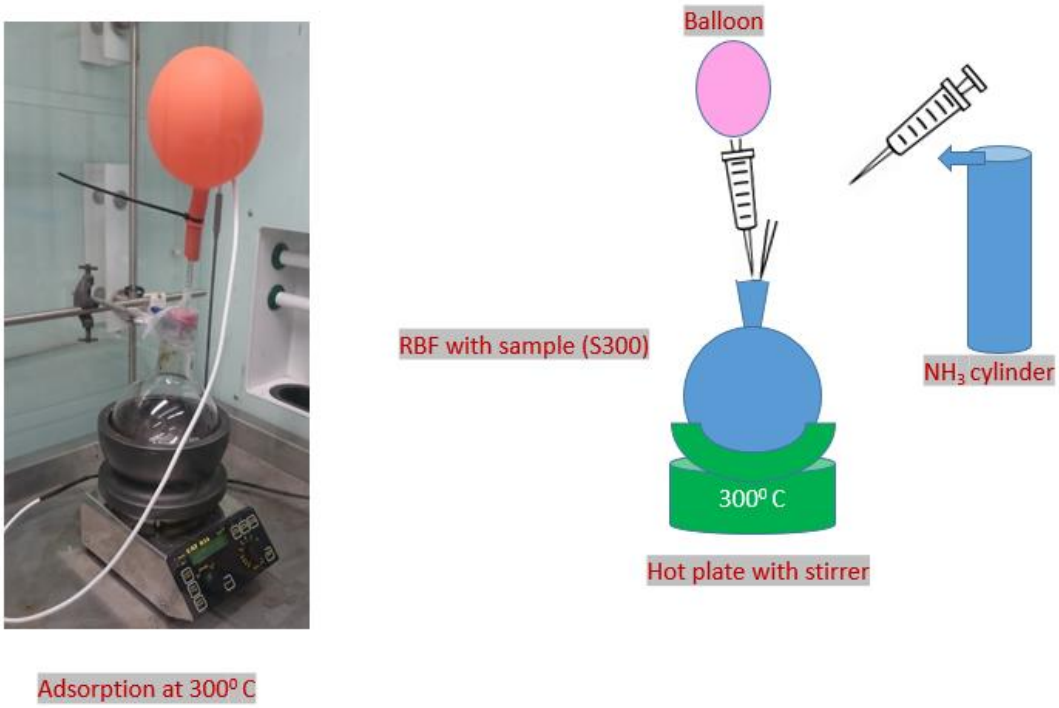

Figure 45. RBF method of generating N-doped materials

- STA method: approx. 10mg of expanded starch is heated up to 625˚C in STA625 with 10˚C/min, in presence of ammonia. Desorption is performed in presence of N_2.

2.4.2. Characterisation of new n-doped materials

In attempt to interpret the chemistry of the n-doped materials, A625 (from expanded alginic acid heated up to 625°C in presence of ammonia, in STA625) was analysed.

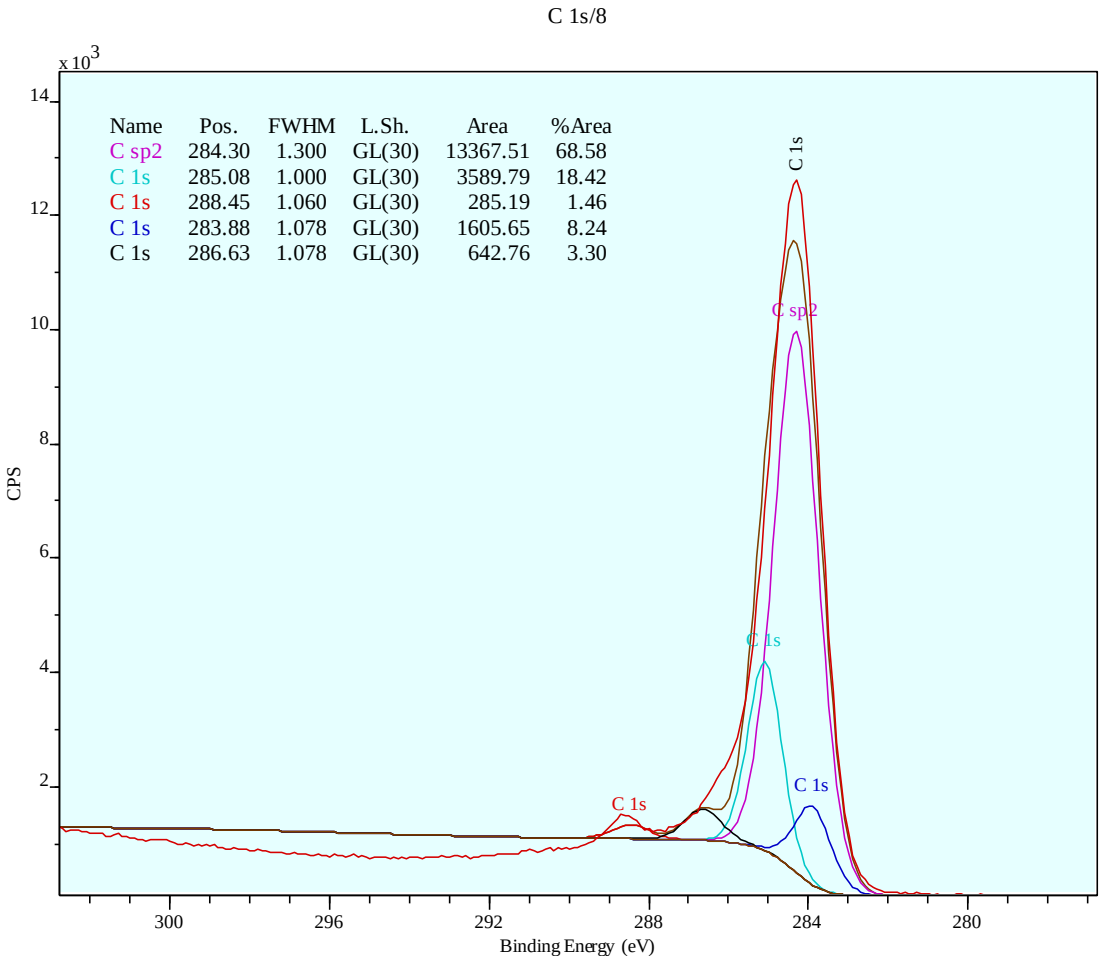

Figure 46. XPS analysis. De-convolution of the C 1s spectrum of expanded alginic acid modified by gaseous NH_3 at 625 ℃ (A625 is the final product)

The XPS spectrum of A625+NH_3 (Fig 46) showed 5 peaks in the C1s region; 284.3 eV (graphitic, sp2), 285.08 eV (non-functionalised sp3), 283.88 eV, 286.63 eV (nitrile) and 288.45 eV (carbonyl, amide).

The N1s region showed 3 peaks (Fig 47): 398.08 eV (imines), 399.98 eV (nitriles, amines) and 399.08 (amines) eV.

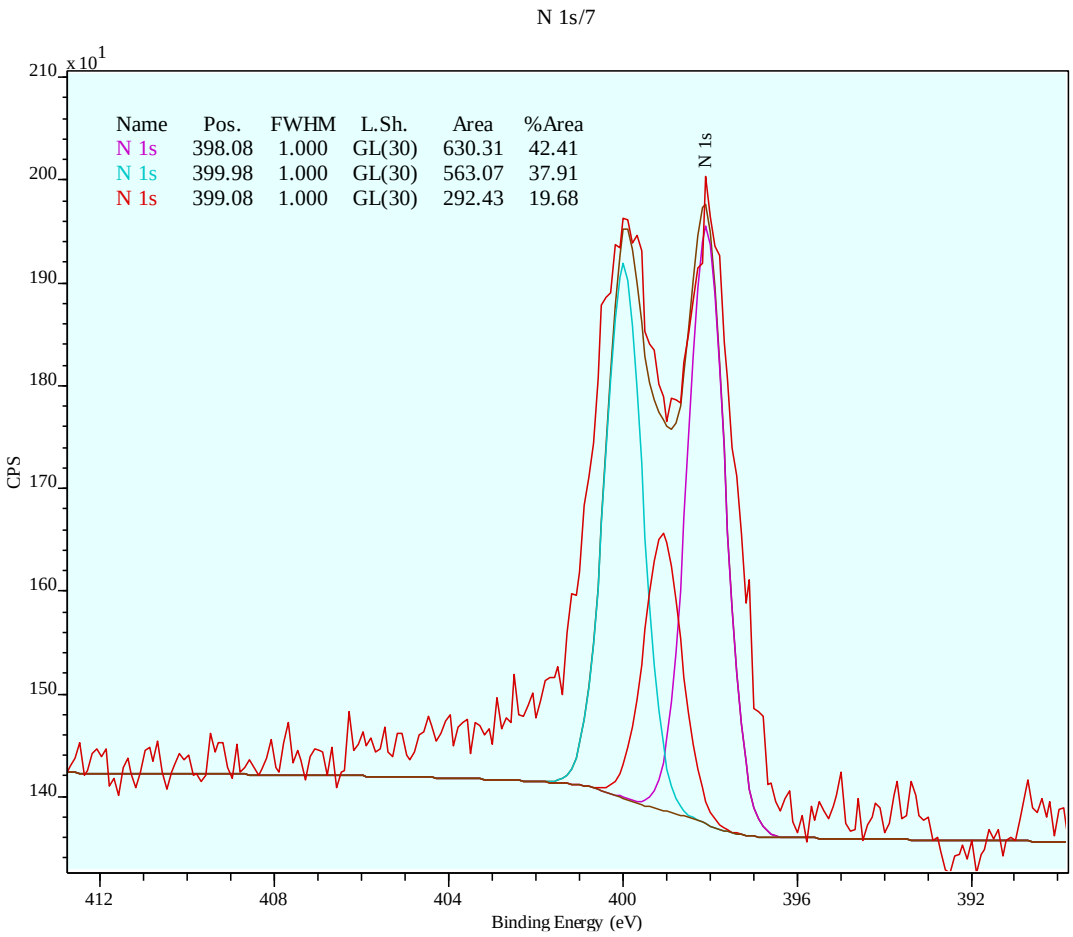

Figure 47. XPS analysis. De-convolution of the N 1s spectrum of expanded alginic acid modified by gaseous NH_3 at 625 ℃

Using the RBF method (heating the Starbon® in a round bottom flask to 300°C in presence of ammonia), nitrogen content of up to 17 % was achieved in the bulk (CHN analysis in Fig 48, bottom), but the total pore volume and micropore volume decreased and mesopore volume and pore size increased. The n-doped materials are still porous (Fig 48, top) which is believed to make them good candidates for adsorption of small molecules.

Porosity of new n-doped materials

	BET m^2/g	Pore vol cm^3/g	Micro-pore vol cm^3/g	Meso-pore vol cm^3/g	Pore size nm
Initial S300	354	0.594419	0.069843	0.524576	11.4448
S300+NH3(RBF method)	114	0.580756	0.007429	0.573327	12.8602

CHN analysis

	%C	%H	%N	%rest
Initial S300	67.4	3.8	0.2	28.6
S300+NH3(RBF method)	54.4	2.6	17.2	25.7

Figure 48. Textural properties and elemental analysis of new n-doped materials

The XPS spectrum of S300+NH_3 (Fig 49) showed 5 peaks in the C1s region; 284.3 eV (graphitic, sp2), 284.74 eV (non-functionalised sp3), 285.89 eV (amine, imine), 287.1 eV (nitrile) and 288.16 eV (carbonyl, amide). The N1s region showed 3 peaks; 398.62 eV (pyridinic, imines), 399.76 eV (nitriles, amines) and 400.61 (amides) eV. The nitrogen content was found about 12% on surface (Table 6) for this material.

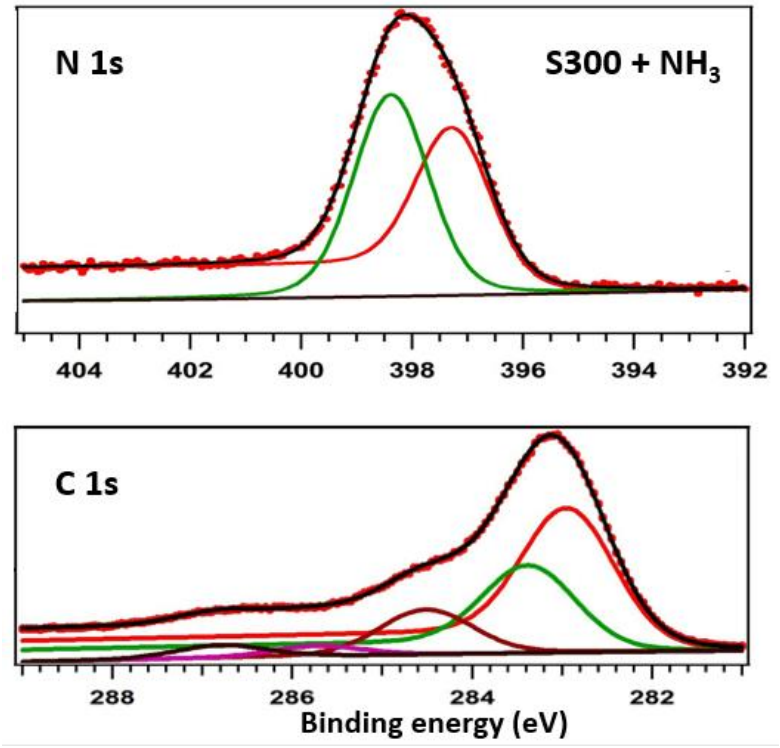

Figure 49. XPS analysis. De-convolution of the N 1s and C 1s spectra of S300 modified by gaseous NH_3 at 300℃

The presence of nitriles is given by DRIFT too, at 2224 cm^{-1}(Fig 50):

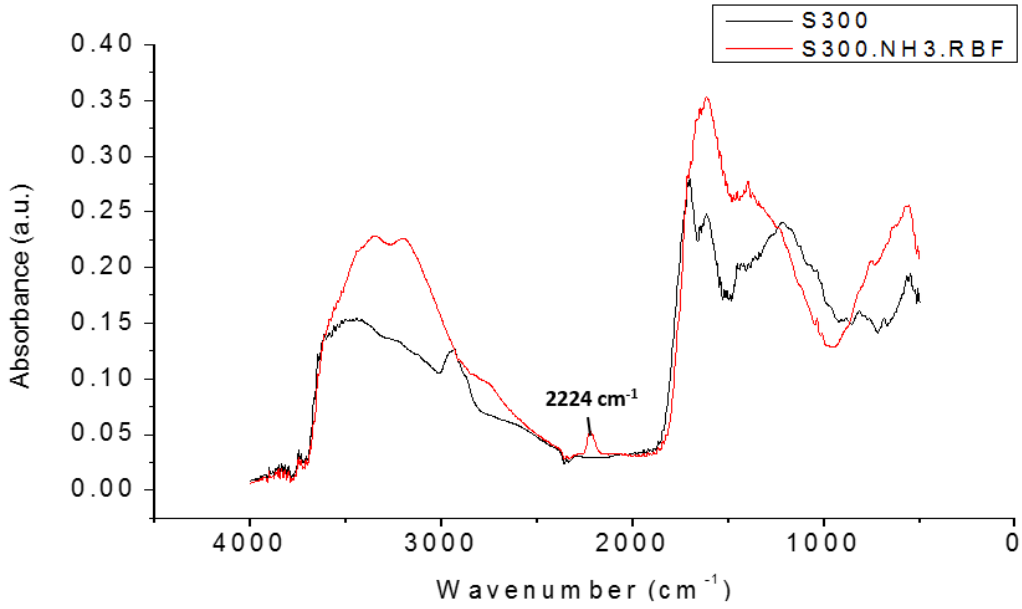

Figure 50. DRIFT-FTIR analysis of initial S300 and n-doped S300 and the presence of nitriles in n-doped material at 2224 cm^{-1}

The temperature when the nitriles form was studied. If in the past their presence was noticed at high temperatures (600-900˚C) and it represent an area of real interest.

Expanded alginic acid was heated to different temperatures in presence of NH_3 (2ml NH_3/min, heating rate 10˚C/min, in STA). The first time when the nitriles (2215 cm^{-1}) were present in DRIFT spectra (1:100 conc. of material in KBr) it was at 230˚C in a small concentration. The nitriles became more visible at 240˚C and the biggest concentration was recorded for carbonization temperature at 350˚C.Thus comparing the intensity of nitriles peak with another peak of the same spectrum would probably give some information about which of S300 or S350 would absorb more ammonia.

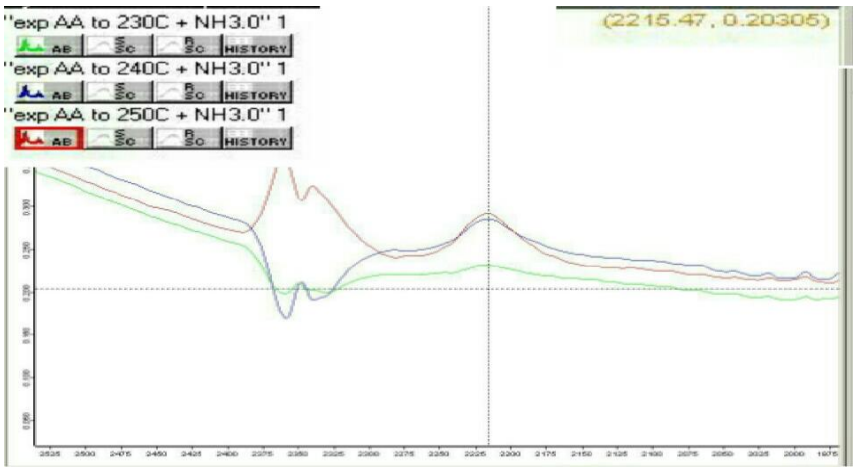

Figure 51. DRIFT-FTIR spectra of expanded materials heated to 230, 240 and 250C in presence of ammonia with peak position at 2215.47 cm^{-1}

The same experiment was proceeded for S300 heating to different temperatures in presence of ammonia. In this case the nitriles were first recorded at 180˚C in small concentration and more visible with the increase of temperature with a peak for nitriles at 2227 cm^{-1} (Fig 52):

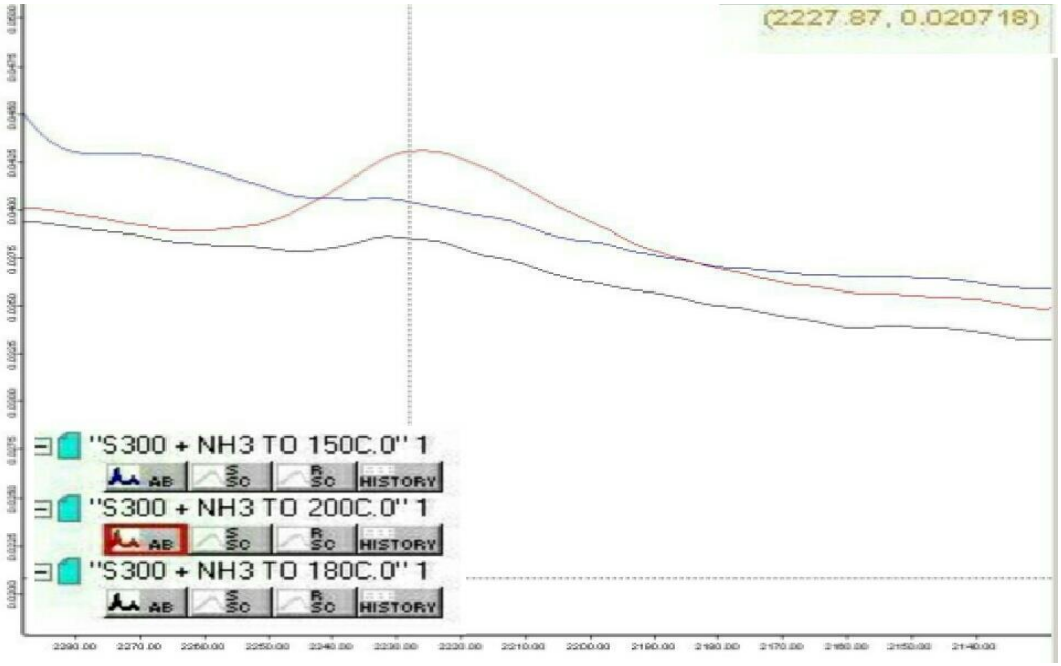

Figure 52. DRIFT-FTIR spectra of S300 heated to 150, 170 and 200C in presence of ammonia with peak position at 2227 cm-1

The expanded alginic acid forms nitriles at higher temperature than S300 because it needs to reach at least 200˚C to form carboxylic groups first which then react with ammonia. S300 already has the acidic groups on its surface and the amination takes place earlier.

3. Experimental Procedure

3.1. Materials

The materials used in this project are biomass as a feedstock and greener chemicals and simple processes, respecting the Green Chemistry rules highlighted previously.

3.1.1. Biomass

The main chemicals present in biomass are: biopolymers (e.g. chitin/chitosan, starch, cellulose, hemicellulose and lignin), oil/fat, protein, sugars and secondary metabolites (essential oils, waxes, pharmaceuticals, antioxidants, pigments).

During this project a number of 4 biomass-derived materials have been produced: Starbon®, Algibon, Starch-derived Monolith and Starbon-graphene.

Two different biomasses were used in this study: starch and alginic acid.

Starch, is the second most abundant biopolymer on earth (after cellulose) and is a naturally occurring polysaccharide found in green plants. Its two main components are polymers of glucopyranose units: amylose is a largely linear molecule of α-(1-4) linked units and amylopectin, similar but around 5% of the base units also have an α-(1-6) link and so the molecule is branched.[49] The amylose is responsible for solubility in hot water with swelling, forming starches.

Green products from starch include: biodegradable plastics, super absorbents starches used in hygiene, stabiliser of emulsions in paint, binder in fertilisers used in agrochemicals, adhesives and glues.[85,86]

Starch is stored in plants as compact micro-granules partly crystalline and water-insoluble in a highly ordered structure by hydrogen bonding of amylose and amylopectin molecule. Because starch has many OH groups, starch is very hydrophilic. Swelling, hydration and solubilisation of the starch granules is caused by H_2O molecules penetrating into the starch granule during the gelatinisation process. Once modified through expansion and partial carbonisation these structures provide a porous material with a highly functionalised surface which can be used for both adsorption and catalysis.

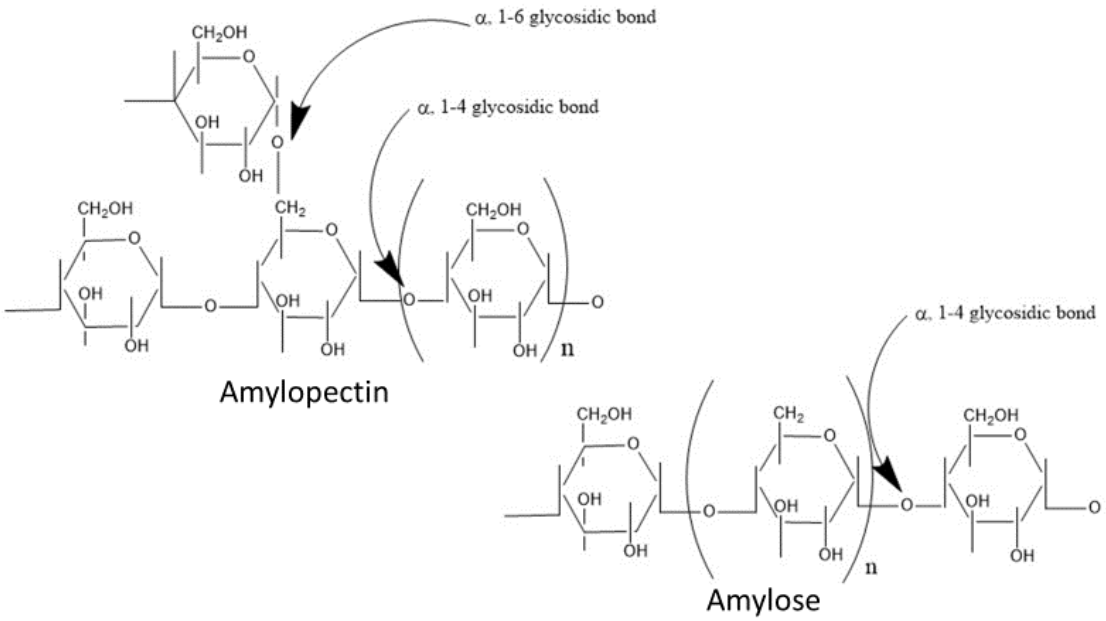

Figure 53. The structure of amylose and amylopectin

The starch used in the project is a corn starch HYLON VII PCR from ''Ingredion ANZ Pty Ltd '', white powder which changes the colour while carbonizing at 100°C in pale yellowish or brown-black when carbonised at higher temperatures.

Alginic acid is a high molecular weight linear polymer from seaweed, consisting of a linear β-1→4-linked polymer of n-mannuronic and L-guluronic acid, shown in Fig 54. This product is approximately 61% mannuronic acid and 39% guluronic acid.

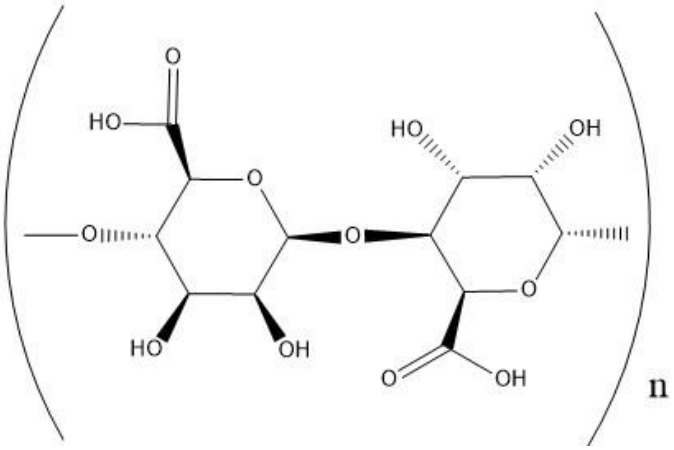

Figure 54. The structure of alginic acid from brown algae

Alginic acid is used in processed foods, pharmaceuticals (as an excipient combined with aluminum hydroxide and magnesium carbonate to form antiacids[87]), textile manufacturing, animal feed and cosmetics. Alginic acid can also be found as the salt sodium alginate which has a high affinity for metal binding especially $Cu^{2+,}$ Ca^{2+}, Zn^{2+} and Pb^{2+}. The

carboxylic acid sites have been shown to directly increase the level of metal adsorption in aqueous systems.[88]

Commercial alginic acid was purchased from Sigma Aldrich (now Merck).

3.1.2. Reagents and solvents

Chemicals used for this study were sourced as follows: *p*-Toluenesulfonic acid monohydrate (≥ 98.5%, Aldrich), *t*-Butanol (TBA, ≥99.0%, Aldrich), graphene nanoplatels (6-8 nm thick x 5 microns wide, Strem Chemicals, Inc).

Absolute ethanol and acetone were purchased from VWR Chemicals ®.

Deionised water was provided in-house by the lab using an ELGA CENTRA® system.

Activated Carbon CarboTech PAK D 700 S was purchased from CarboTech.

Ammonia cylinder for this study was borrowed from Teaching Labs of Chemistry Department, University of York.

CO_2 cylinder was purchased from BOC.

3.2. Equipment

The textural properties, EA, STA, infrared spectroscopy were carried out using the facilities belonging to the Department of Chemistry, University of York, UK.
TEM section and SEM section were carried out at Bioscience Technology Facility, Biology Dept, University of York.
XPS analyses were carried out at The School of Engineering and Materials Science Queen Mary, University of London and NEXUS- Newcastle University.

3.2.1. Furnaces and ovens

Carbonisation of expanded biomass was carried out in a Barnstead Thermolyne6000 furnace under the vacuum at different temperatures, according to the Starbon® preparation method.
Carbonisation of dyed expanded starch is done in a Barnstead Thermolyne6000 furnace under the vacuum at different temperatures, according to Starbon preparation method.

Gelation was performed in a CEM MARS6 microwave using Easy Prep Plus vessels, control type -ramp to 140°C for over 10 min. The gel is prepared from a mixture of starch: water in proportion of 10g starch:70ml water.

For graphene materials a smaller scale microwave has been used, Discover, using the following rates of heating:

1. RT-100°C, 5°C/min, holding time 1h
2. 100°C-210°C, 0.3°C/min, holding time 1h
3. 210°C-400°C, 0.3°C/min
4. 400°C-600°C, 1°C/min
5. 600°C-800°C and higher, 3°C/min.

3.2.2. STA625

The unique setup based on STA625 has designed and contracted to investigate adsorption of gas molecules such as water and CO_2 on the surface of porous materials. Simultaneous TGA-DSC measures both heat flow (Differential Scanning Calorimetry) and weight changes (thermogravimetric) in Starbon® as a function of temperature or time in a controlled atmosphere.

The installation of adsorption used in our experiments includes: the STA625, 2 bottles (one with water and one used as trap), CO_2 cylinder (Fig 55).

In ***CO_2 adsorption***, the CO_2 comes from the cylinder, goes to the flowmeter, into the trap and using a tap to adjust the flow it goes into the STA.

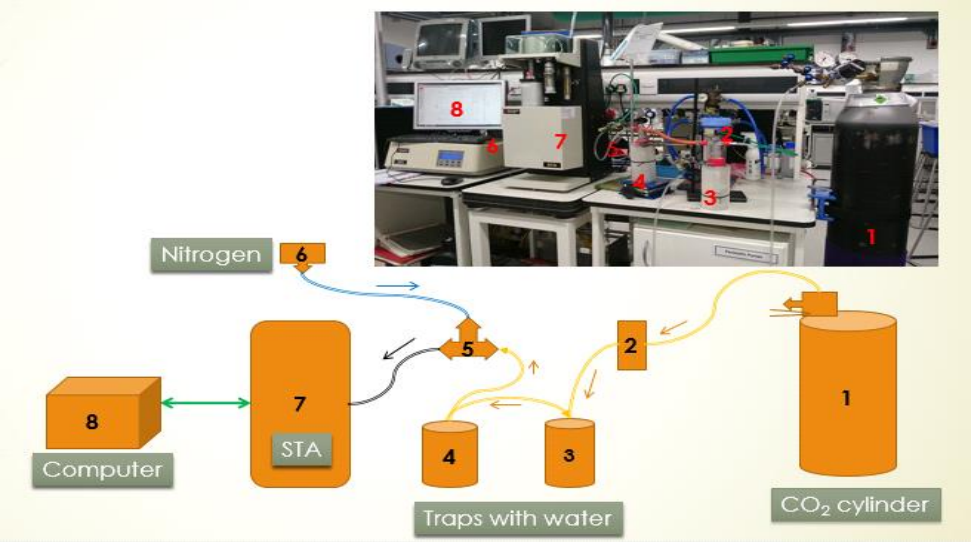

Figure 55. The installation used in CO_2/CO_2+H_2O

In case of ***water adsorption***, the N_2 was bubbling through the water in the first bottle. The nitrogen saturated with water vapour was passed through the trap to avoid any drops of water to be injected into the STA chamber (Figure 56). The yellow arrows show the H_2O+N_2 flow, magenta is for pure N_2 flow and the pink arrows shows the path of CO_2 through the system.

Figure 56. The water traps used in CO_2+H_2O adsorption

The system used in ammonia study is presented in Fig 57 and includes: STA625, computer, a syringe for the gas and nitrogen source:

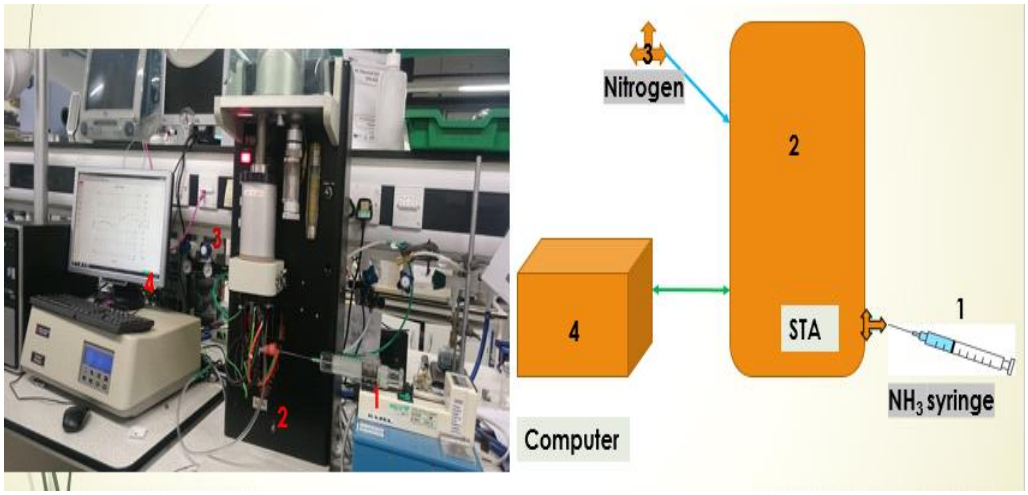

Figure 57. The installation used in ammonia adsorption

3.2.3. Freeze dryer

The drying of expanded starch is carried out on a VirTis SP Scientific freeze dryer, using the inner chamber, under -60°C and 50 mTorr for a good vacuum. The expanded starch is treated with TBA after retrogradation and cooled down with liquid nitrogen before drying.

3.2.4. Centrifuge

Solent exchange is done using Heraeus Megafuge 40R Centrifuge using the follow method: 20°C, for 30 min, 3000 rpm.

3.3. Analytical methods

3.3.1. ASAP2020

Nitrogen-physisorption adsorption measurements were carried out at 77 K using a Micromeritics ASAP 2020 volumetric adsorption analyser for the characterisation of surface property of materials. The specific surface area measured in this work was that recognised by the nitrogen molecule. Before measuring, the powdered samples (0.5g) were dried under vacuum for 4 h at 40°C for the white powders and 4h at 140° C for the black ones. Analysis of pore distribution has been done by standard procedures,[89,90,91] MP method proposed by Mikhail et al.[89] was used for evaluation of microporous sample volumes and the Barret–Joyner–Halenda (BJH) equation[90] was used for volume of

mesopores and pore-size distribution of the Starbon® materials. The characteristic energy of adsorption $E_{surface}$ was calculated from Dubinin–Radushkevich adsorption isotherm equation.[91]

3.3.2. FTIR Spectroscopy

ATR-FTIR The functional groups present in the Starbon® samples were investigated using PerkinElmer Spectrum 400 FT-IR/FT-NIR Spectrometer with transmittance peaks in 4000-650 cm^{-1} region, with rapid scanning (4 scans) and resolution 4 cm^{-1} at room temperature.

DRIFT spectrum were recorded using an EQUINOX 55 FTIR spectrometer (BRUKER). The absorbance peaks were recorded in the 4000–500 cm^{-1} region of the infrared spectrum, 256 scans for the background and 128 for the samples, resolution 1 cm^{-1} at room temperature.

3.3.3.TEM and SEM images

S300 5%graphene for TEM imaging will have been suspended in ethanol and a few microlitres put on a grid with formvar/carbon support film. They will have been images at 120kV with Tecnai 12 BioTWIN, scale bar on the images.

Samples used for SEM imaging (starch 5%graphene, S300 5%graphene, graphene) were mounted on sticky tabs and sputter coated with gold/palladium, around 7nm. The images with just a scale bar were taken on the JEOL JSM-6390LV, at 8kV.

Both TEM and SEM section were done by Meg Stark from Bioscience Technology Facility, Biology Department, University of York.

3.3.4. XPS analysis

The XPS analysis were carried out by Professor Maria-Magdalena Titirici from The School of Engineering and Materials Science, Queen Mary, University of London and David Morgan from National EPSRC XPS Users Service (NEXUS) on an AXIS Nova instrument.

4. Conclusions

Mesoporous carbons provided superior CO_2 adsorption properties to microporous AC. Thermodynamic measurements indicate that CO_2 is captured by a physisorption mechanism which involves both direct and indirect (through mesopores) access to the micropores within the material. This opens a new approach to design micro/meso porosities for CO_2 adsorption. The process is rapidly reversible without requiring large energy input, so that CO_2 capture and release can occur under pressure swing rather than temperature swing conditions. The enthalpy of CO_2 adsorption on the high temperature Starbons® are similar to that of Norit activated carbon suggesting that the adsorption mechanisms are the same and that the role of the mesopores is to make more micropores accessible to CO_2.

Starbon-graphene composites developed the highest CO_2 adsorption, improving Starbon's adsorption performance and could be taken in consideration in future for other adsorption processes.

It has been shown that Starbons adsorbed NH_3 by both physisorption and chemisorption mechanism.

Based on ammonia chemisorption process a novel method of synthesis of n-doped materials has been developed. The maximum loading of 17% of nitrogen was acheved at the conditions: high temperature (up to 300°C) in presence of pure ammonia gas. Lower temperature was found to generate nitrile groups.

It has been shown that surface functionality of the n-doped Starbon cosists of amide, amine and nitrile groups and this opens a new approach in designing good adsorbers for CO_2 and other small polarisable compounds.

Appendix

The results and data analysis methods of this study are presented separately as a spreadsheet (Microsoft Excel format). The spreadsheet is not protected and all cells can be edited.

Table 1. Textural properties of polysaccharide-derived composites used in CO_2 adsorption

T_p /^{0}C	S_{BET} (m^2/g)	V_{total} (cm^3/g)	$V_{mesopore}$ (cm^3/g)	$V_{micropore}$ (cm^3/g)	Average pore radius (nm)
S300	187.1964	0.257565	0.218411	0.039154	8.6699
S450	489.8374	0.666743	0.549853	0.11689	8.9011
S650	623.3036	0.614066	0.424045	0.190021	9.9337
S800	773.8439	0.677858	0.417355	0.260503	10.4965
S1000	895.7833	0.927977	0.693032	0.234945	8.9794
S1200	650.3356	0.797358	0.64058	0.156805	9.8953
S800 5%graphene	565.5548	0.677133	0.483066	0.194067	16.2208
A300	140.3011	0.643566	0.643566	-0.004689	9.7579
A550	499.0695	0.852517	0.747688	0.104829	6.8373
A800	689.1967	0.961733	0.814575	0.147158	5.8508
A1000	480.8283	0.96296	0.840061	0.122899	13.2023
A1200	340.3101	1.006475	0.956916	0.049559	13.1697
AC	786.331	0.650023	0.493911	0.156112	4.0464

Table 2. Textural properties of graphene and graphene-materials

Sample	BET surface m^2/g	Pore volume cm^3/g	Micropore vol cm^3/g	Mesopore vol cm3/g	Pore diameter nm
Exp starch + 1%graphene	60.656	0.397957	0.019599	0.378358	27.9309
Exp starch+ 5%graphene	12.7426	0.052001	-0.003711	0.052001	8.5574
S300 1%	187.0723	0.326265	0.046794	0.279471	14.4787
S300 5%	341.609	0.663377	0.081983	0.581394	15.6089
S800 1%	635.3274	0.312674	0.214911	0.097763	7.336
S800 5%	565.5548	0.677133	0.194067	0.483066	16.2208
Graphene	134.2072	0.117654	0.011547	0.106107	3.3925

Table3. Textural properties of starch-derived composites and monolith form of Starbon

Sample	**BET surface m^2/g**	**Pore volume cm^3/g**	**Micropore vol cm^3/g**	**Mesopore vol cm3/g**	**Pore diameter nm**
Exp starch solv exchange	46.8296	0.306167	-0.003619	0.306167	9.2695
Exp starch sulf method	**14.8268**	**0.181289**	**0.012244**	**0.169045**	**38.292**
Exp starch freeze drying	111.5845	0.679524	0.020284	0.65924	11.2045
S100	96.5799	0.582314	0.014196	0.568118	10.6317
S350	488.6889	0.323156	0.134439	0.188717	6.0379
S300	187.1964	0.257565	0.039154	0.218411	8.6699
S450	489.8374	0.666743	0.11689	0.549853	8.9011
S550	675.7072	0.766697	0.223764	0.542933	14.0024
S800	773.8439	0.677858	0.260503	0.417355	10.4965
S1000	895.7833	0.927977	0.234945	0.693032	8.9794
S1200	650.3356	0.797358	0.156805	0.640553	9.8953
M300	502.1514	0.640782	0.105912	0.53487	7.5248
M800	631.7618	0.29238	0.239766	0.052614	7.9724

Table 4. Textural properties of alginic acid composites and activated carbon

Sample	BET surface m^2/g	Pore volume cm^3/g	Micropore vol cm^3/g	Mesopore vol cm3/g	Pore diameter nm
Expanded Amylose	152.1262	1.055919	0.007472	1.048447	12.2095
Expanded Alginic Acid	83.0877	0.448361	-0.000284	0.448361	8.5109
AC Norit	786.331	0.650023	0.156112	0.493911	4.0464
Exp AA	106.3748	0.416804	-0.006456	0.416804	5.7599
A100	80.1259	0.36241	0.007639	0.354771	5.915
A300	140.3011	0.643566	-0.004689	0.643566	9.7579
A550	499.0695	0.852517	0.104829	0.747688	6.8373
A800	689.1967	0.961733	0.147158	0.814575	5.8508
A1000	480.8283	0.96296	0.122899	0.840061	13.2023
A1200	340.3101	1.006475	0.049559	0.956916	13.1697

Table 5. Elemental analysis (CHN) of starch- and alginic acid derivatives, activated carbon and graphene

T_p/^{0}C	**%C**	**%H**	**%N**	**%rest**	**C:O ratio**	**%Ash**	**%rest after ash**	**C:O ratio final**
S000	41.4	6.3	-	52.3	0.8			
S100	42.1	6.1	-	51.8	0.8			
S300	70.4	3.3	-	26.3	2.7	5.2	21.1	3.3
S450	76.8	3.4	0.2	19.6	3.9			
S550	82.1	2.1	0.2	15.6	5.3			
S650	82.6	1.6	0.2	15.6	5.3			
S800	88.4	0.9	0.1	11.6	7.6	2.8	8.8	10
S1000	77.7	1.7	0.3	20.3	3.8			
S1200	83.9	1	0.2	14.9	5.6			
A000	35.5	4.9	-	59.6	0.6			
A100	36.6	4.5	-	58.9	0.6			
A300	63.4	3.4	0.2	33.5	1.9	14.6	18.9	3.4
A550	79.5	2.3	0.2	18	4.4			
A800	82.2	1.6	0.2	16	5.1			
M300	65.7	2.7	-	31.6	2.1	3.6	28	2.3
M800	80.051	1.558	-	18.395	4.35			
AC	70.2	1.1	1.2	27.5	2.6			
graphene	90.7	0.4	-	8.9	10.2			

Table. 6 XPS quantification of S300 and S300 after ammonia treatment

Sample	Conc O 1s%	Conc C 1s%	Conc N 1s%	Conc other%
S300	**O 1s**	**C 1s**	**S 2p**	
%Conc	21.48	78.18	0.34	
S300 NH3	**O 1s**	**C 1s**	**N 1s**	**S 2p**
%Conc	15.26	72.65	11.61	0.48

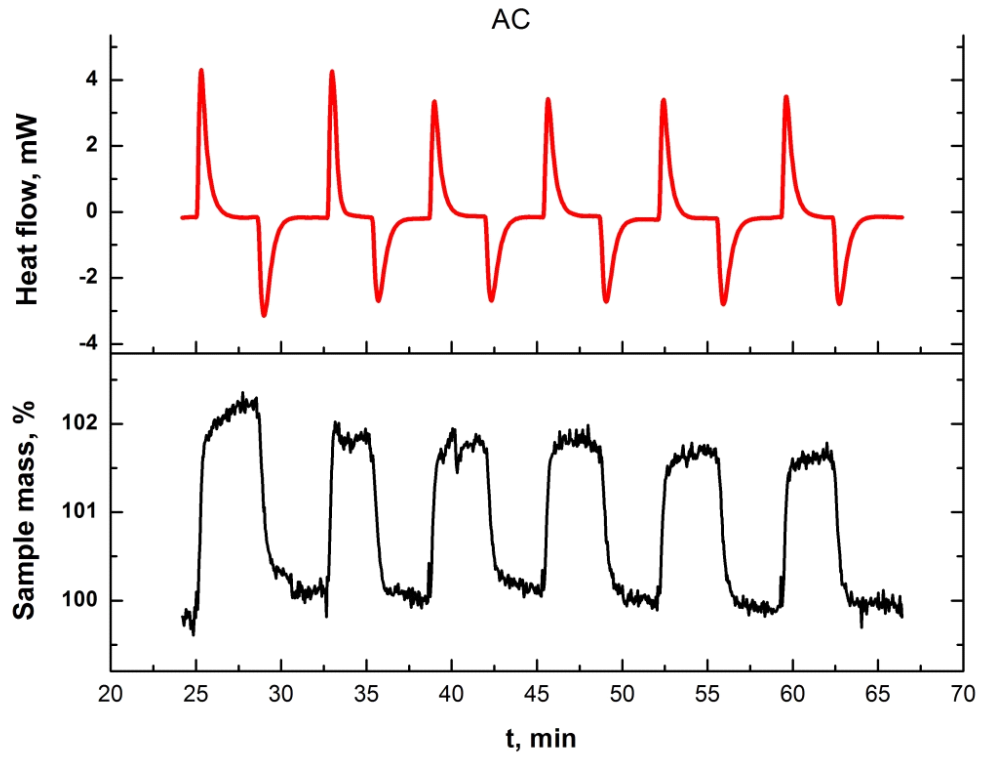

Figure 58. Mass and heat flow change during CO_2 adsorption and desorption using AC at 35 ℃

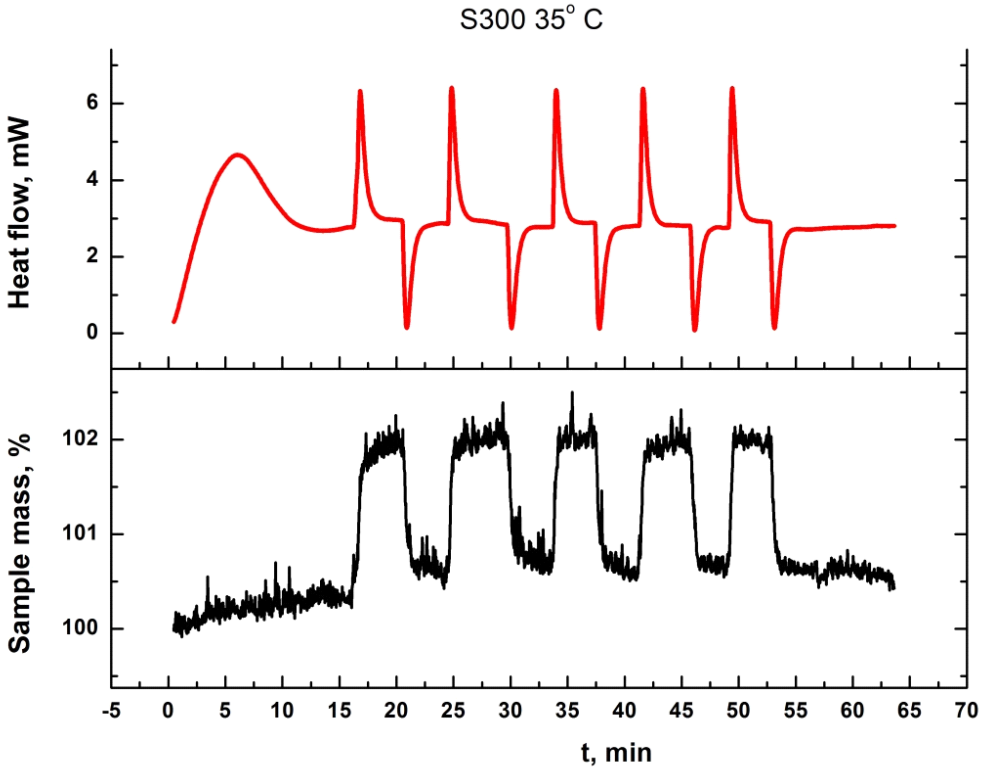

Figure 59. Mass and heat flow change during CO_2 adsorption and desorption using S300 at 35 ℃

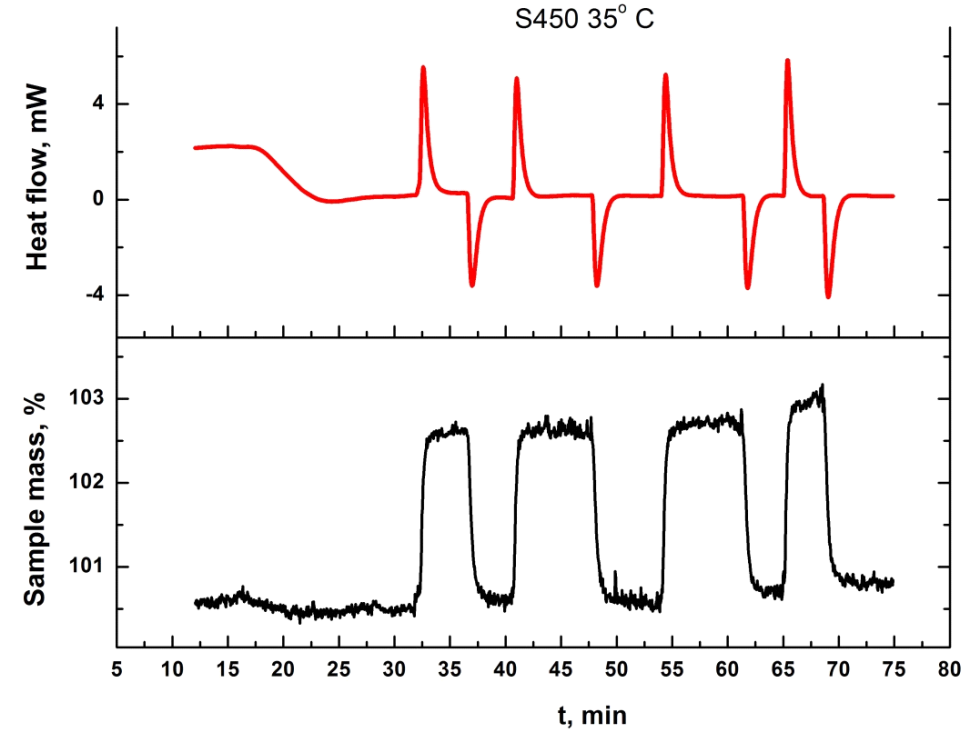

Figure 60. Mass and heat flow change during CO_2 adsorption and desorption using S450 at 35 ℃

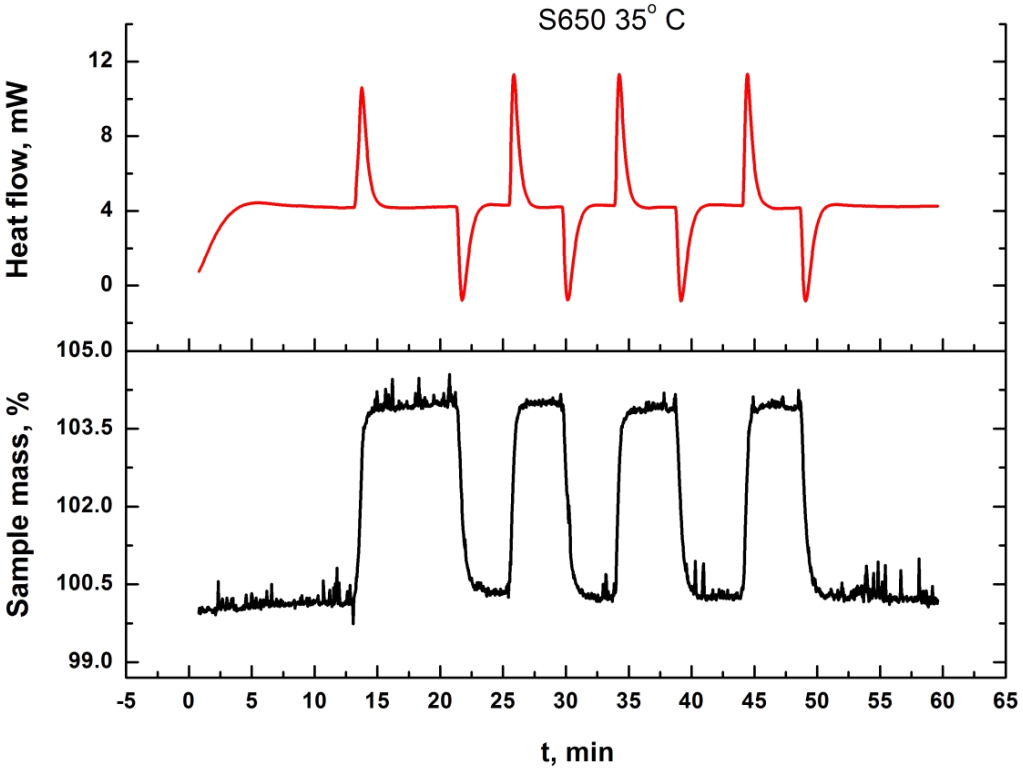

Figure 61. Mass and flow change during CO_2 adsorption and desorption using S650 at 35 ℃

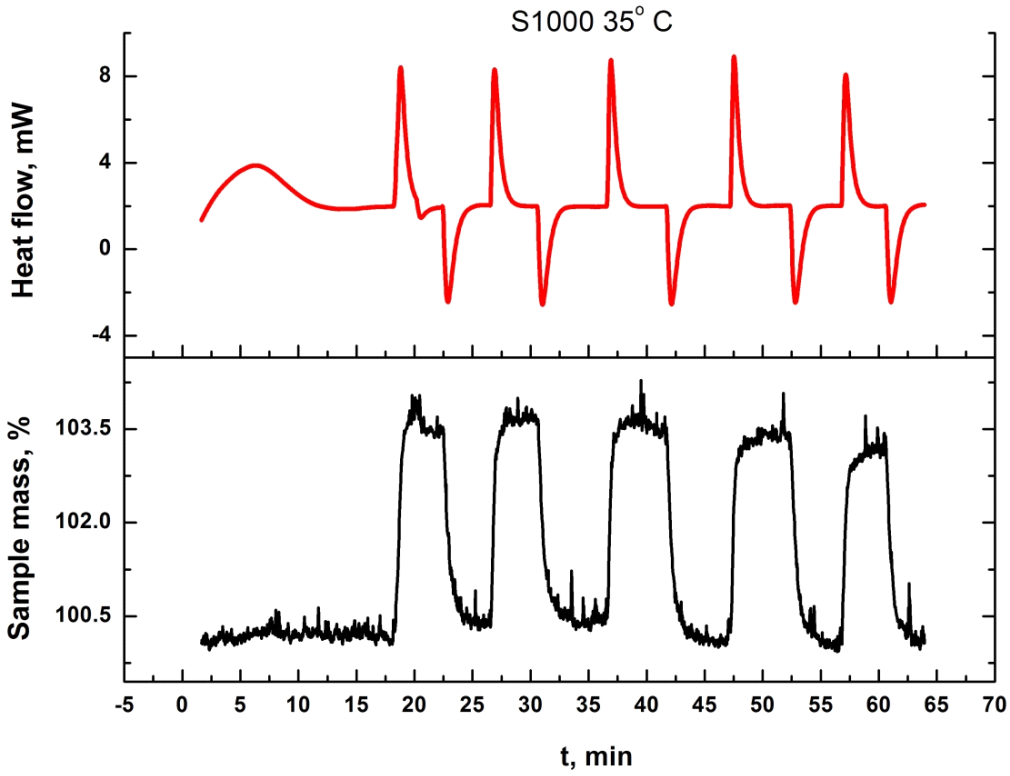

Figure 62. Mass and flow change during CO_2 adsorption and desorption using S1000 at 35 ℃

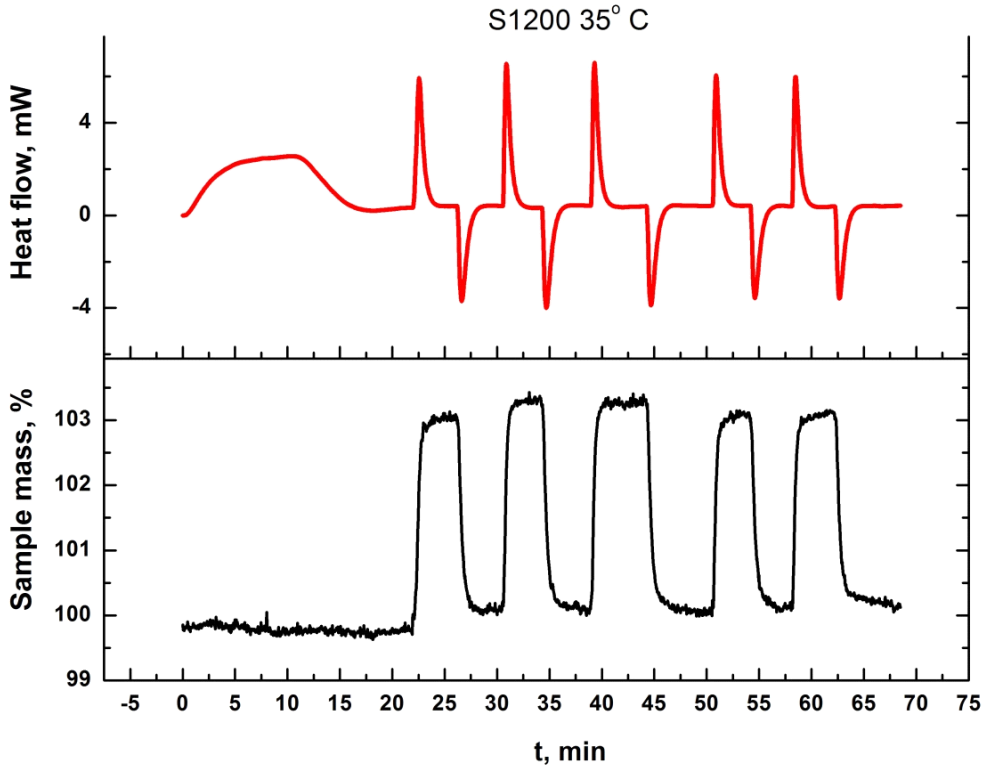

Figure 63. Mass and heat flow change during CO_2 adsorption and desorption using S1200 at 35 ℃

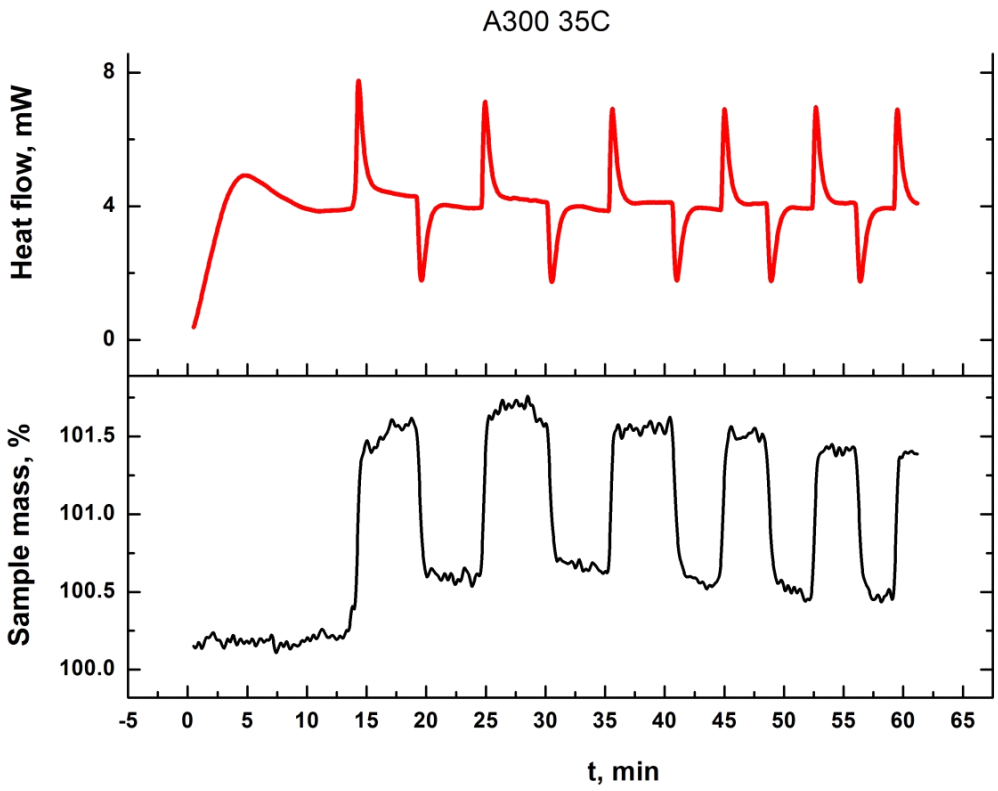

Figure 64. Mass and heat flow change during CO_2 adsorption and desorption using A300 at 35 ℃

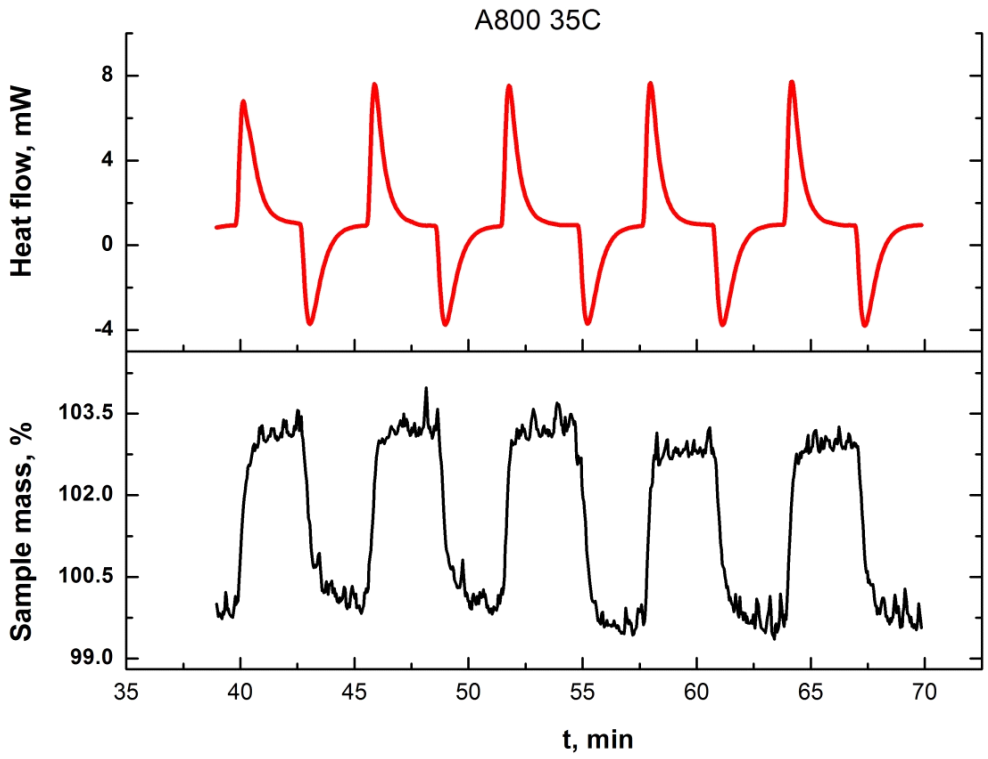

Figure 65. Mass and heat flow change during CO_2 adsorption and desorption using A800 at 35 ℃

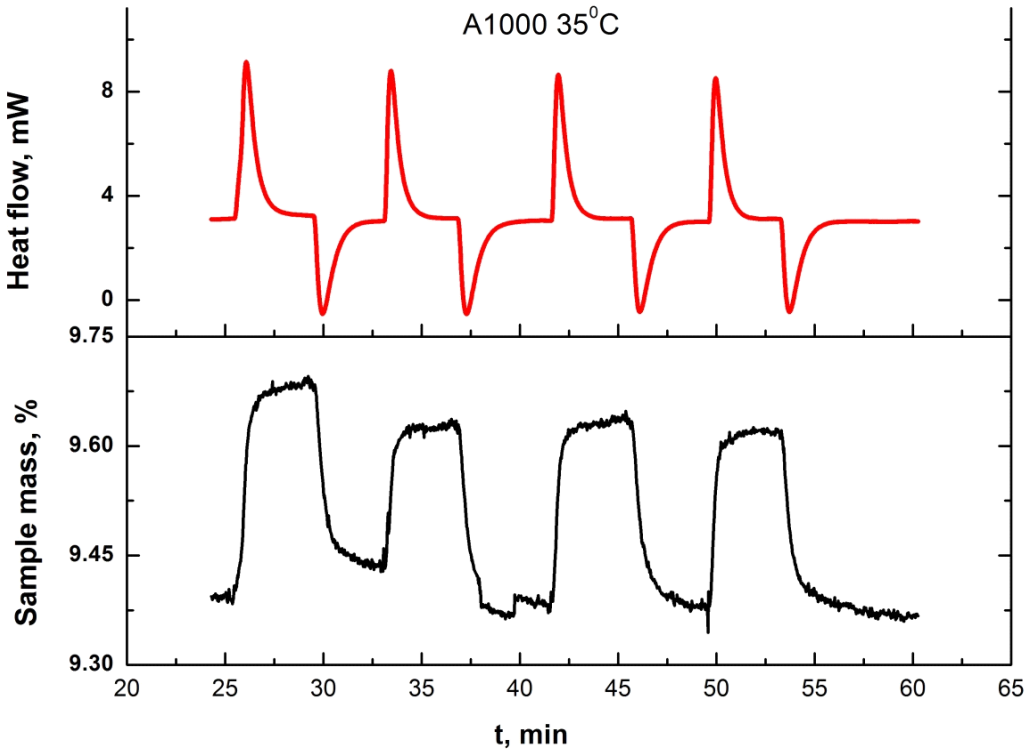

Figure 66. Mass and heat flow change during CO_2 adsorption and desorption using A1000 at 35 ℃

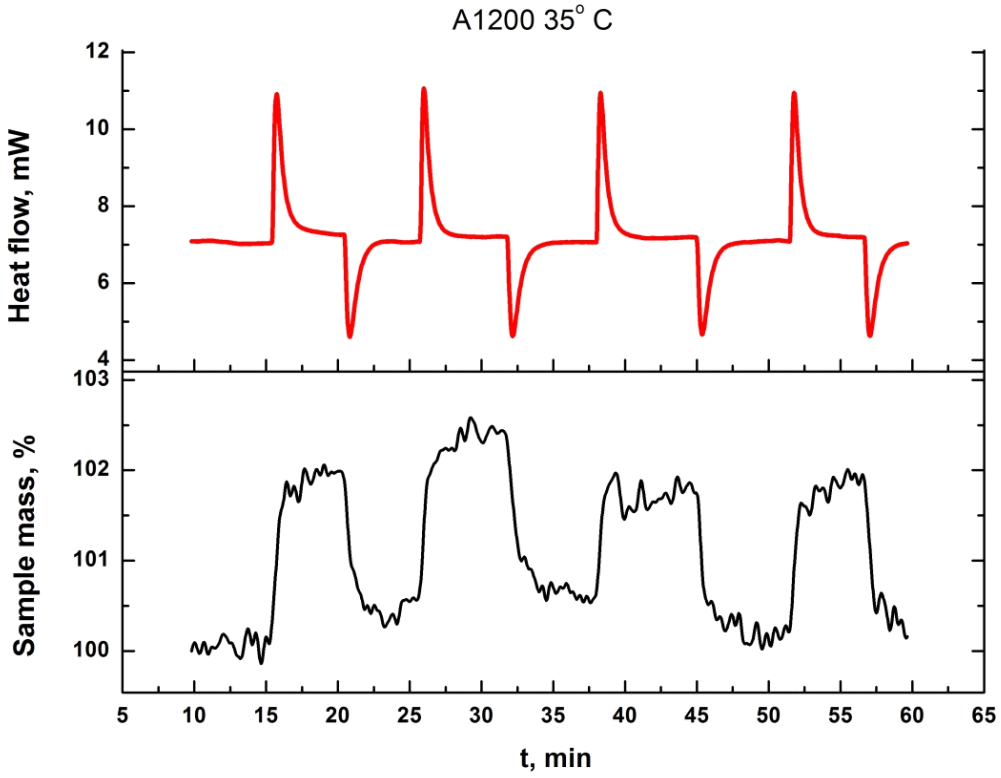

Figure 67. Mass and heat flow change during CO_2 adsorption and desorption using A1200 at 35 ℃

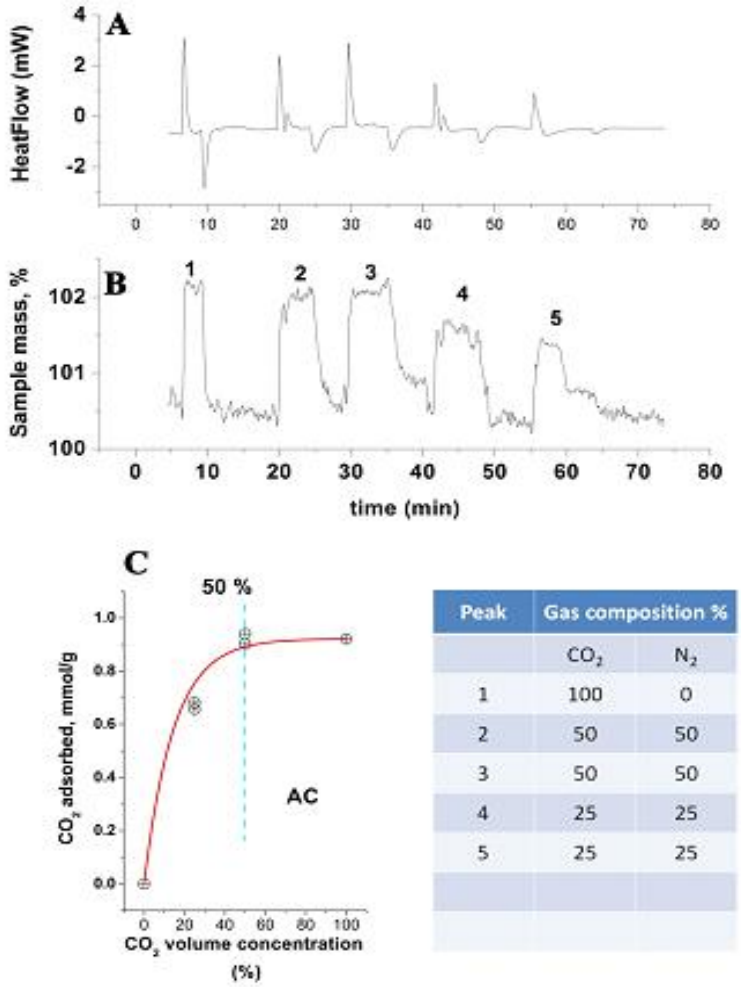

Peak	Gas composition %	
	CO_2	N_2
1	100	0
2	50	50
3	50	50
4	25	25
5	25	25

Figure 68. Influence of gaseous CO_2/N_2 mixture using AC

A800

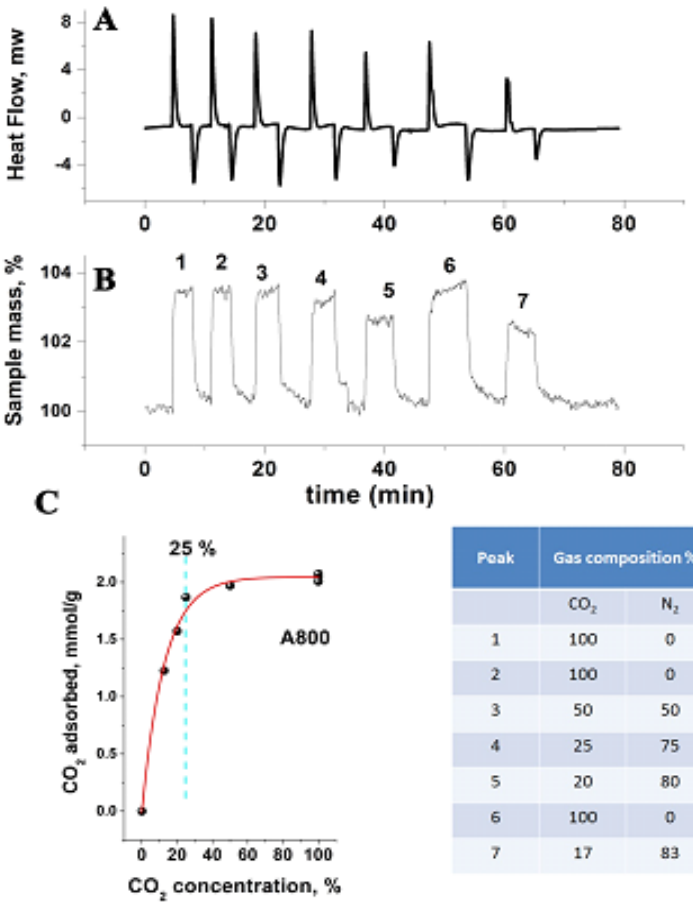

Peak	Gas composition %	
	CO_2	N_2
1	100	0
2	100	0
3	50	50
4	25	75
5	20	80
6	100	0
7	17	83

Figure 69. Influence of gaseous CO_2/N_2 mixture using A800

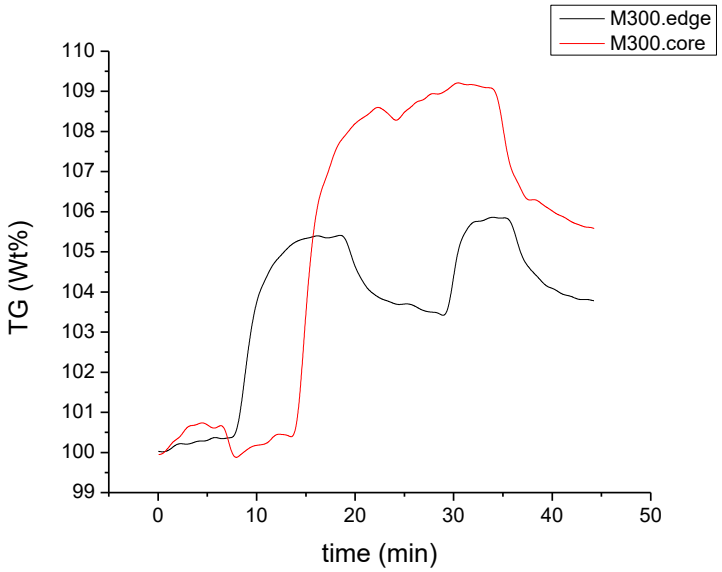

Figure 70. Mass and flow change of ammonia adsorption and desorption of M300 (edge and core) at 35 ℃

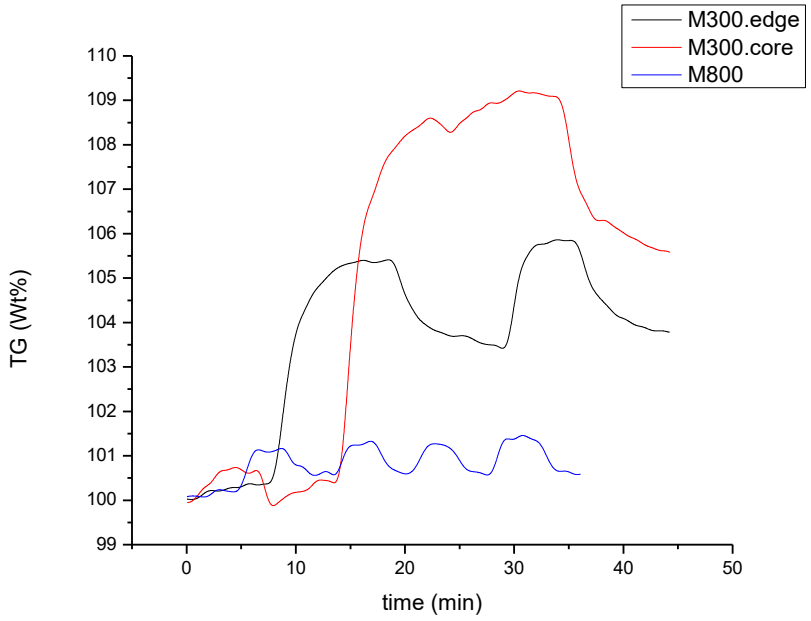

Figure 71. Mass and heat flow change of ammonia adsorption and desorption using M300 (core and edge) and M800

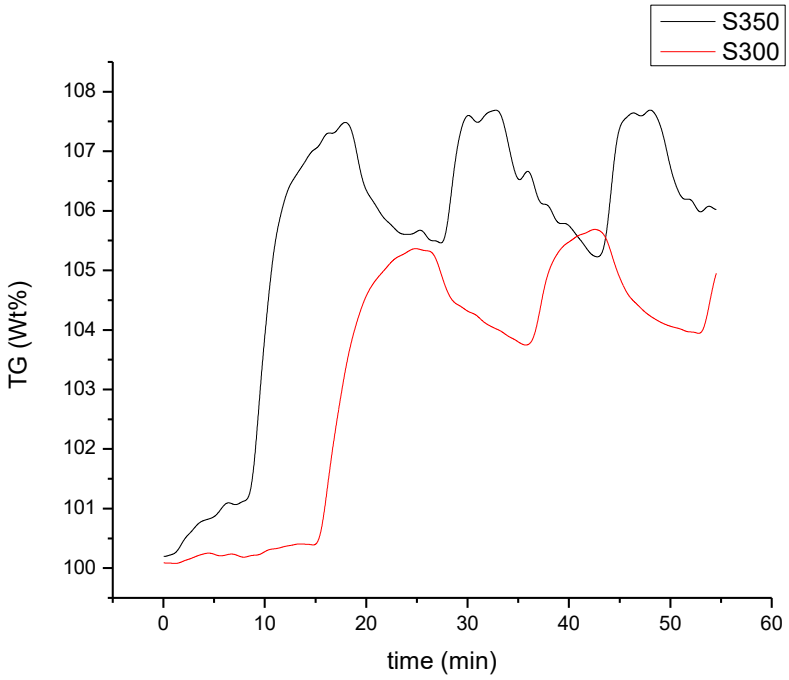

Figure 72. Mass change during ammonia adsorption and desorption using S300 and S350 at 35 ℃

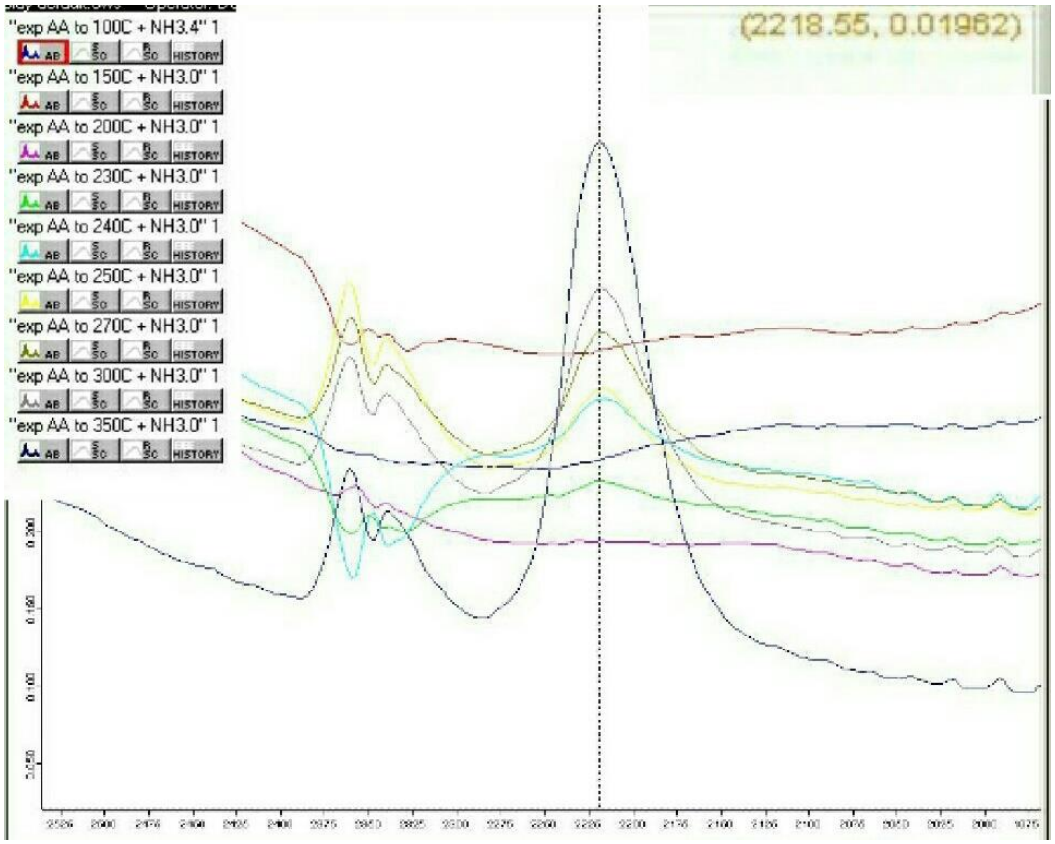

Figure 73. DRIFT-FTIR of expanded alginic acid after heated in presence of ammonia at different temperatures: 100,150, 200,230,240,250,270,300 and 350 ℃

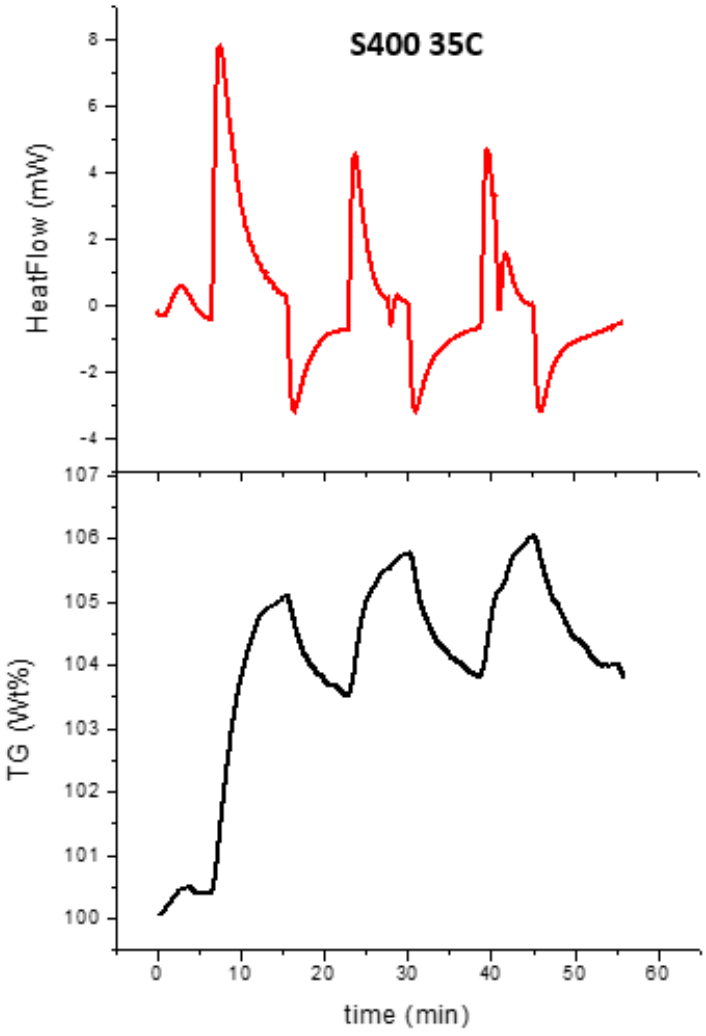

Figure 74. Mass and heat flow change of adsorption and desorption of NH_3 using S400 at 35 ℃

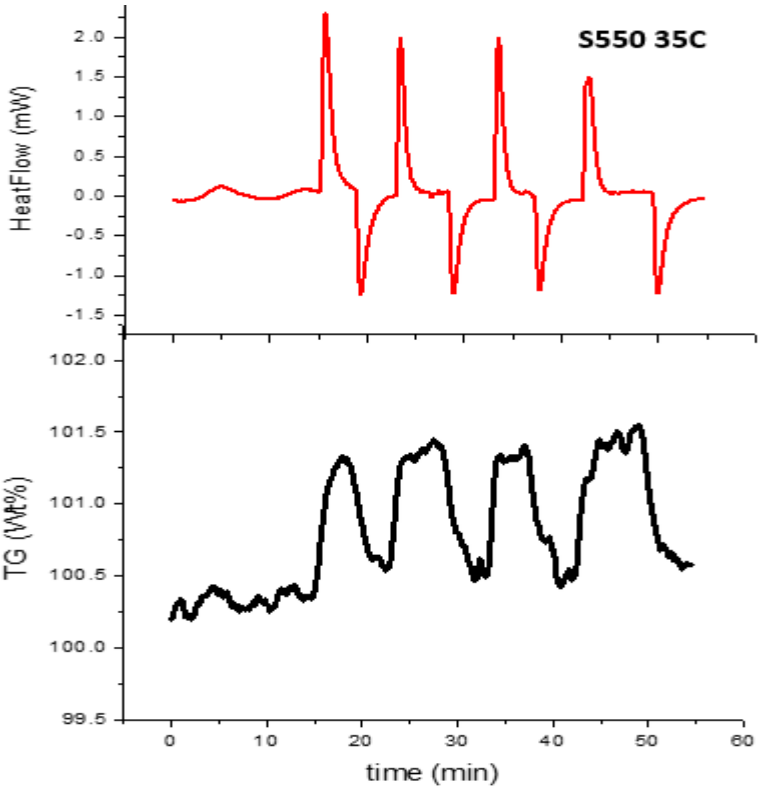

Figure 75. Mass and heat flow of adsorption and desorption of ammonia using S550 at 35 ℃

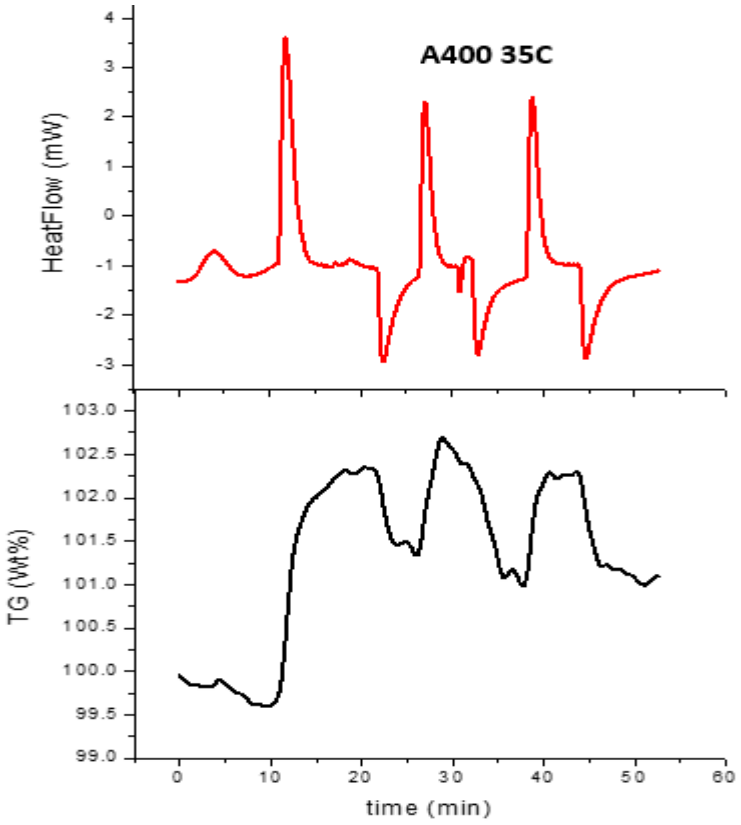

Figure 76. Mass and heat flow change during NH_3 adsorption and desorption using A400 at 35 ℃

Abbreviations

The following abbreviations are used in the text in addition to the periodic table symbols:

A000 - Expanded alginic acid (100,300,550,800 – Algibon at different temperatures of carbonisation)

Ads. - Adsorption

Aq. Gel - Aqua gel

ASAP2020 - ASAP (Accelerated Surface Area and Porosimetry) 2020 System

ATR-FTIR - Attenuated total reflectance Fourier transform infrared spectroscopy

BET - Brunauer, Emmett, Teller

BJH - Barrett, Joyner, Halenda

CHN - Elemental analysis on carbon, hydrogen and nitrogen

Chemi. - Chemisorption

Des. - Desorption

DRIFT - Diffuse reflectance infrared Fourier transform

DSC - Differential scanning calorimetry

EA - Elemental (CHN) Analyser

eV - Electron volt

Exp. - Expanded (i.e. starch, algibon)

FTIR - Fourier transform infra-red

IR - Infrared Spectroscopy

IUPAC - International union for pure and applied chemistry

MP - Micropore analysis method

MPa - Mega pascal

mw - Molecular weight

NMR - Nuclear magnetic resonance

P - Pressure

PD - Pore diameter

Physi. - Physisorption

p-TSA - p-Toluene Sulfonic Acid

PV - Pore volume

RBF - Round bottom flask

RT - Room temperature

S000 - Expanded starch (100,300,50,800 Starbons® at different temperatures of carbonisation

SA - Surface area

SEM - Scanning Electron Microscopy

S_{BET} - Specific surface area

STA - Simultaneous Thermal Analysis

T - Temperature

TBA - Tert-Butyl Alcohol

TEM - Transmission Electron Microscopy

TGA - Thermogravimetric analysis

T_p - Temperature of Starbon preparation

VOCs - Volatile Organic Compounds

XPS - X-ray photoelectron spectroscopy

References

1. J. Sharaf, *International Journal of Engineering Research and Applications*,2013, **3**, 947-960.
2. National Research Council, *Rethinking the Ozone Problem in Urban and Regional Air Pollution.* National Academy Press, Washington, DC, 1991.
3. J. A. Logan, *Journal of Geophysical Research-Atmospheres*, 1985, **90**, 10463-10482.
4. S. E. Schwartz, *Science*, 1989, **243**, 753-763.
5. R. Atkinson, *Atmospheric Environment*, 2000, **34**, 2063-2101.
6. J.F. Pankow, *Atmospheric Environment*, 1987,**21**,2275-2283.
7. T.F. Bidleman, *Atmospheric processes.* Environmental Science and Technology, 1988, **22**,361-367.
8. J.R. Odum, T. Hoffmann, F. Bowman, D. Collins, R.C. Flagan, J.H. Seinfeld, *Environmental Science and Technology*, 1996, **30**, 2580-2585.
9. J.R. Odum, T.P.W. Jungkamp, R.J. Griffin, R.C. Flagan, J.H. Seinfeld, Science, 1997, **276**, 96-99.
10. L. Cao, G. Bala, K. Caldeira, R. Nemani and G. Ban-Weiss*, Proceedings of the National Academy of Sciences of the United States of America,* 2010, **107**, 9513–9518.
11. https://www.youtube.com/watch?v=iC7drcAyuA8 .
12. M.G. Plaza, C. Pevida, B. Arias, J. Fermoso, A. Arenillas, F. Rubiera, J.J. Pis, Journal of Thermal Analysis and Calorimetry, 2008, **92**, 601–606.
13. A. Arenillas, K.M. Smith, T.C. Drage, C.E. Snape, *Fuel*,2005, **84**, 2204–2210.
14. C. Pevida, M.G. Plaza, B. Arias, J. Fermoso, F. Rubiera, J.J. Pis, *Applied Surface Science,*2008, **254**, 7165–7172.
15. M.G. Plaza, C. Pevida, B. Arias, J. Fermoso, F. Rubiera, J.J. Pis, *Energy Proceedia*, 2009, **1**, 1107–1113.
16. M. S. Shafeeyan, W.M.A.W. Daud, A. Houshmand, A. Shamiri*, Journal of Analytical and Applied Pyrolysis,*2010, **89**, 143–151.
17. A. Brunetti, F. Scura, G.Barbieri, E.Drioli, *Journal of Membrane Science*,2010, **359**, 115-125.
18. S. Choi, J. H. Drese, C. W. Jones, *ChemSusChem*, 2009, **2**, 796–854.
19. D. M. D'Alessandro, B. Smit, J. R. Long, Angewandte Chemie International, 2010, **49**, 6058–6082.
20. Y.-S. Bae, R. Q. Snurr, Angewandte Chemie International Edition, 2011, **50**, 11586–11596.
21. Q. Wang, J. Luo, Z. Zhong, A. Borgna, *Energy* & *Environmental Science*, 2011, **4,** 42–55.
22. B. P. Spigarelli, S. K. Kawatra, *Journal* of *CO2* Utilization, 2013, **1**, 69–87.
23. Z. Jeirani, C.H. Niu and J. Soltan, *Reviews in Chemical Engineering*, 2016, 1-32.

24. M.Ghaedi, A. Golestani Nasab, S. Khodadoust, M. Rajabi, S. Azizian, *Journal of Industrial and Engineer Chemistry*, 2014, **20**, 2317-2324.
25. C.A. Snyders, C.N. Mpinga, S.M. Bradshaw, G. Akdogan, J.J. Eksteen, *Journal of the Southern African Institute of Mining and Metallurgy*, 2013,113.
26. M.A. Barakat, *Arabian Journal of Chemistry*,2011, **4**, 361-377.
27. J. Altman at all, *Water Air Soil Pollut*, 2015, **226**, 384.
28. Islam MS et al, *Journal* of *Environmental Management*, 2015 ,**152**, 49–57.
29. M.G. Plaza, Pevida, B. Arias, J. Fermoso, M.D. Casal, C.F. Martin, F. Rubiera, J.J. Pis, 2009, *Fuel*, **88**, 2442–2447.
30. W.J. Decker, H.F. Combs, D.G. Corby, *Toxicology and Applied Pharmacology,* 1968, **13**, 454-460.
31. Control of Volatile Organic Compound Emissions from Manufacture of High-Density Polyethylene, Polypropylene, and Polystyrene Resins, Emision standards and Engineering Devision, *U.S. Environmental Protection Agency*,1983, EPA-450/3-83-008.
32. https://www.desotec.com/en/carbonology/carbonology-academy/activated-carbon-gases-and-air-purification.
33. M.N. Rashed, *InTech*,2013, **7**,168-169.
34. E.O. Wiig, S.B. Smith**,** *Journal of Physical Chemistry*, 1951, **55,** 27–44.
35. R.C. Bansal, M. Goyal, Activated Carbon Adsorption, *Science*,2005, 11-16.
36. C.C. Rodrigues, de Moraes D. Jr., da Nobrega S.W, M.G. Barboza*, Bioresource Technology* ,2007, **98**, 886–891.
37. X. Li Long, H. Cheng, Z.L. Xin, W. De Xiao, W. Li, W.K. Yuan, *Wiley InterScience*, 2008,**27**,225–233.
38. R.K. Sinha, N.J. Wagner, R.S. Joyce, *United States Patent*, 1978, **4**, 072,479.
39. C.C. Huang, S.M. Chu, C.H. Chen, *Journal of Hazardous Materials*, 2006, **136**, 866-73.
40. W. Gao, D. Butler, D.L. Tomasko, *Langmuir*, 2004, **20**, 8083– 8089.
41. R.V. Siriwardane, M.S. Shen, E.P. Fisher, *Energy Fuels* ,2005, **19**, 1153–1159.
42. Z. Xiang, D. Cao, J. Lan, W. Wang, D. P. Broom, Energy Environmental Science, 2010, **3**, 1469–1487.
43. J.R. Li, Y. Ma, M. C. McCarthy, J. Sculley, J. Yu, H.K. Jeong, P. B. Balbuena, H.C. Zhou, *Coordination Chemistry Reviews*, 2011, **255**, 1791– 1823.
44. M.G. Plaza, C. Pevida, A. Arenillas, F. Rubiera, J.J. Pis, *Fuel*,2007,**86**, 2204–2212.
45. T.C. Drage, A. Arenillas, K.M. Smith, C. Pevida, S. Piippo, C.E. Snape, *Fuel*,2007, **86**, 22–31.
46. M.M. Maroto-Valer, Z. Lu, Y. Zhang, Z. Tang, *Waste Management Research*, 2008, **28**, 2320–2328.
47. M.M. Maroto-Valer, Z. Tang, Y. Zhang, *Fuel Processing Technology,*2005, **86**, 1487–1502.

48. J. Przepiórski, M. Skrodzewicz, A.W. Morawski, *Applied Surface Science*, 2004, **225**, 235–242.

49. V. Budarin, J. H. Clark, R. Luque, R. White, *Material Matters, 2009,* **4***, 19.*

50. V. Budarin, J.H. Clark, J. J. E. Hardy, R. Luque, K. Milkowski, S.J. Tavener, and A.J. Wilson, *Angewandte Chemie, International Edition*,2006, **45**, 3782–3786.

51. C. T. Kresge, M. E. Leonowicz, W. J. Roth, J. C. Vartuli and J. S. Beck, *Nature*, 1992, **359**, 710-712.

52. D. Zhao, J. Feng, Q. Huo, N. Melosh, G. H. Fredrickson, B. F. Chmelka and G. D. Stucky, *Science*, 1998, **279**, 548.

53. R. White, *Porous Carbon Materials from Sustainable Precursors, Royal Society of Chemistry, 2015*, 53-81.

54. A. Borisova, M. De Bruyn, V. L. Budarin, P. S. Shuttleworth, J. R. Dodson, M. L. Segatto and J. H. Clark, *Macromol Rapid Commun*, 2015, **36**, 774-779.

55. R. White, *Porous Carbon Materials from Sustainable Precursors, Royal Society of Chemistry, 2015*, 156-190.

56. J. Lee, S. Yoon, T. Hyeon, S. M. Oh and K. Bum Kim, *Chemical Communications*, 1999, 2177-2178.

57. J.R. Dodson, H.L. Parker, A.M. García, A. Hicken, K. Asemave, T.J. Farmer, H. He, J.H. Clark and A.J. Hunt, *Green Chem.*, 2015,**17**, 1951-1965.

58. G. Dura, V. Budarin, J.A. Castro-Osma, P.S. Shuttleworth, S.C. Z. Quek, J.H. Clark, and M. North, Angewandte Chemie International Edition, 2016, **55**, 1–6.

59. Y. Gao, X. Chen, J. Zhang and N. Yan, *ChemPlusChem*, 2015, **80**, 1556-1564.

60. Z. R. Ismagilov, A. E. Shalagina, O. Y. Podyacheva, A. V. Ischenko, L. S. Kibis, A. I. Boronin, Y. A. Chesalov, D. I. Kochubey, A. I. Romanenko, O. B. Anikeeva, T. I. Buryakov and E. N. Tkachev, *Carbon*, 2009, **47**, 1922-1929.

61. K. Gong, F. Du, Z. Xia, M. Durstock and L. Dai, *Science*, 2009, **323**, 760.

62. M. Li, F. Xu, H. Li and Y. Wang, *Catalysis Science & Technology*, 2016, **6**, 3670-3693.

63. M-M. Titirici, R. J. White, N. Brun, V.L. Budarin, D.S. Su, F. del Monte, J.H. Clark and M.J. MacLachlang, *Chemical Society Reviews*, 2015,**44**, 250-290 .

64. P. T. Anastas, J.C. Warner, Green Chemistry Theory and Practice*, Oxford University Press*, 1998,30.

65. PAC*, Pure and Applied Chemistry,*1976*, **46**,* 79.

66. C.F. Poole, The Essence of Chromatography, *Elsevier,***1st edition***,* 2003.

67. A. Sayari, *Chemistry of Materials*, 1996, **8**, 1840.

68. S.H. Joo et al., *Nature*, 2001, ***412***, 169.
69. V.L. Budarin, J.H. Clark, J.J.E. Hardy, R. Luque, K. Milkowski, S.J Tavener, and A.J. Wilson, *Angewandte Chemie International Edition*,2006, **45**, 3782–3786.
70. R. Fu, L. Liu, W. Huang, P. Sun, *The Journal of Applied Polymer Science*, 2003,**87**,2253 – 2261.
71. S. Jeong, C. Werth, *Environmental Science Technology*, 2005,**39**, 3279 –3288.
72. K. Kim, W. Regan, B. Geng, B. Alemán, B. M. Kessler, F. Wang, M. F. Crommie and A. Zettl, *Physsica Status Solidi*, 2010, **11**, 302–304.
73. http://webbook.nist.gov/cgi/cbook.cgi?ID=C124389&Mask= 4#Thermo-Phase.
74. K. H. Yung, *Journal of Physical Chemistry*, 1995, **99**, 12021–12024.
75. http://webbook.nist.gov/cgi/cbook.cgi?ID=C124389&Mask= 4#Thermo-Phase.
76. V.L. Budarin, R. Luque, J.H. Clark, D.J. Macquarie, A. Koutinas, *Green Chemistry*, 2007,**9**,992-995.
77. C.S.K. Lin, R. Luque, J.H. Clark, C. Webb and C. Du, *Energy Environmental Science*, 2011,**4**, 1471-1479.
78. P.S. Shuttleworth, V.L. Budarin, S.W. Breeden, D.J. Macquarrie, R.L. Luque, R. White, J.H. Clark, STARBONS®: Preparation, applications and transition from laboratory curiosity to scalable product, *Clean Technology*, 2011, 267 – 270.
79. M. Li, F. Xu, H. Li and Y. Wang, *Catalysis Science & Technology*, 2016, **6**, 3670-3693.
80. Y. Gao, X. Chen, J. Zhang and N. Yan, *ChemPlusChem*, 2015, **80**, 1556-1564.
81. Z. R. Ismagilov, A. E. Shalagina, O. Y. Podyacheva, A. V. Ischenko, L. S. Kibis, A. I. Boronin, Y. A. Chesalov, D. I. Kochubey, A. I. Romanenko, O. B. Anikeeva, T. I. Buryakov and E. N. Tkachev, *Carbon*, 2009, **47**, 1922-1929.
82. K. Gong, F. Du, Z. Xia, M. Durstock and L. Dai, *Science*, 2009, **323**, 760.
83. B.J. Meldrum and C.H. Rochester, *Journal* of the *Chemical Society*, *Faraday Transactions*, 1990, **86**, 1881-1884.
84. B. Stöhr, H. P. Boehm and R. Schlögl, *Carbon*, 1991, **29**, 707-720.
85. V. Budarin, J. H. Clark, R. Luque, R. White, *Material Matters, 2009,* **4***, 19.*
86. V. Budarin, J.H. Clark, J. J. E. Hardy, R. Luque, K. Milkowski, S.J. Tavener, and A.J. Wilson, *Angewandte Chemie, International Edition*,2006, **45**, 3782–3786.
87. https://www.drugs.com/mtm/alginic-acid-aluminum-hydroxide-and-magnesium-carbonate.html.
88. T.A. Davis, B. Volesky and A Mucci, *Water Research,* 2003,**37**,4311-4330.
89. R. S. Mikhail, S. Brunauer, E. E. Bodor, *Journal of Colloid and Interface Science,* 1968, ***26***,45–53.

90. E. P. Barrett, L. G. Joyner, P. P. Halenda, *Journal of the American Chemical Society,* 1951, ***73***, 373–380.
91. P. J. Reucroft, W. H. Simpson, L. A. Jonas, *Journal of Physical Chemistry,* 1971, ***75***,3526–3531.